NASA CR-132557

FINAL REPORT ON THE MANUFACTURE AND STATIC FIRING OF X259-E6 ROCKET MOTOR SERIAL NUMBER XJ04/0001

NASA Contract NAS1-10000-R80

Prepared by
D. Ray Robertson
Hercules Incorporated
Bacchus Works Magna, Utah

NASA CR-132557

FINAL REPORT ON THE MANUFACTURE AND STATIC FIRING OF X259-E6 ROCKET MOTOR SERIAL NUMBER XJ04/0001

By D. Ray Robertson

Prepared under NASA Contract NAS1-10000 Task R80
Hercules Incorporated
Bacchus Works, Magna, Utah
Via LTV Aerospace Corporation Purchase Order No. P-832479-AER

for

Langley Research Center
National Aeronautics and Space Administration

TABLE OF CONTENTS

LIST OF FIGURES

LIST OF FIGURES (Cont)

LIST OF FIGURES (Cont)

LIST OF TABLES

FINAL REPORT ON THE MANUFACTURE AND STATIC FIRING OF X259-E6 ROCKET MOTOR SERIAL NUMBER XJ04/0001

By D. Ray Robertson
Hercules Incorporated
Bacchus Works Magna, Utah

SUMMARY

A single motor was cast and static fired to demonstrate the performance of high energy crosslinked double base (XLDB) propellant in standard X259 rocket motor hardware. Prior to motor fabrication, the motor was comprehensively analyzed to predict the results of static firing the X259 motor loaded with XLDB propellant. As a result of the analyses, a forward dome shrinkage liner was added to the design. With this design change it was determined that adequate margins of safety existed.

The motor, designated the X259-E6 model with serial number XJ04/0001, was fabricated using a slurry-casting technique and was assembled with a standard X259-B4 nozzle which had the nozzle throat machined to a smaller inside diameter than the B4 model and the exit cone cut short for Bacchus Works altitude expansion.

The motor was static fired on 20 February 1974 with the nozzle failing during motor operation. Nozzle failure was attributed to spalling of the throat material leading to complete nozzle break-up. However, the propellant functioned as predicted in the motor chamber, ignition was normal, and char and erosion of the internal insulator were as expected.

Omission of the specific type of XLDB propellant is intentional to allow this report to be unclassified.

INTRODUCTION

The Antares II motor (X259) is the third stage of the NASA Scout vehicle. The object of this program was to demonstrate high energy crosslinked double base propellant (XLDB) at sea level conditions in standard X259 hardware to provide greater capability for the Scout vehicle. Maximum performance gain with minimum hardware design changes was the primary goal.

MOTOR ANALYSES

Engineering motor analyses were performed on the X-259-E6 demonstration motor as reported in Engineering Analyses for X259-E6 (Antares II-B) with Demonstration Propellant, 30 August 1973 and revised December 1973, Letter No. X259/6/40-4031 and as updated in the following paragraphs.

Effect of OPC Rate Data

The heat-transfer sensitivity analysis used in the above-referenced analyses was applied to the modified X259 nozzle to determine the effects of the actual XJ04/0001 propellant lot, based on one pound charge (OPC) rate data, on the predicted thermal stresses. The OPC rate data led to an average X259 chamber pressure prediction of 463 psia (319.01 N/cm^2) compared to 590 psia (406.79 N/cm^2) from the referenced analyses and a burn time of 31.5 seconds compared to 27.0 seconds from the referenced analyses, a 16.7 percent increase.

It was assumed that the decreased chamber pressure correspondingly decreased the convective coefficient by the following proportion:

$$h_2 = h_1 \left(\frac{P_2}{P_1}\right)^{0.8} = h_1 \left(\frac{463}{590}\right)^{0.8} = h_i\ (0.824) \qquad (1)$$

Equation (1) indicates that the time-average convective coefficient was decreased throughout the nozzle by 17.6 percent using the OPC rate data. From Figure 7-1 of the referenced analyses, a 10 percent decrease in the convective coefficient results in a surface temperature change of approximately 0.4 percent in the X259 exit cone. Therefore a 17.6 percent decrease will result in approximately an 0.7 percent decrease in the surface temperature and thus the decrease in chamber pressure will have an insignificant effect on the margins of safety shown in Tables XIII, XIV, and XV of the referenced analyses.

Figure 7-2 of the referenced analyses was used to approximate the change in bulk temperature of the nozzle due to the increased (OPC rate) burn time. Figure 7-2 indicates that the temperature at the backside of exit cone graphite phenolic will increase approximately 4.4 percent for a 10 percent increase in burn time. Using this location for an approximate measure of the bulk temperature, the 16.7 percent increase in burn time will result in approximately a 7.4 percent increase in the bulk temperature. This slight increase in the bulk temperature will result in some increases and some decreases in the end-of-burn margins of safety of Tables XIII, XIV, and XV in the referenced analyses. The 7.4 percent increase in bulk temperature will, however, increase the stresses in the tables by no more than 7.4 percent. Therefore, to be conservative, all stresses at 27 seconds in the tables were increased by 7.4 percent. Strengths are also temperature

dependent, but most of the maximum stress occurred in cool regions and this effect was neglected. Other than the exit cone overwrap, the minimum margin calculated was 0.72. This is higher than the 0.31 at 20 seconds which would remain the minimum regardless of burn time. The 0.08 margin of safety in the exit cone overwrap at 27 seconds was decreased to 0.01, however the strength used considered only hoop wraps of glass when in actuality two layers of glass cloth are used and the actual axial strength of the overwrap is considerably greater than the 4000 psi (2757.9 N/cm^2) used.

It was concluded that the modified X259 nozzle would perform satisfactorily considering the X259 propellant lot OPC rate data.

Effect of Propellant Lot Actual Mechanical Properties

Propellant mechanical properties from the mix loaded into the X259-E6, XJ04/0001 were compared with properties used in the structural analyses. The data are from recast dogbones and dogbones machined from the X259 casting column. The comparison of properties is given in Table I. The measured mechanical properties fall within the lower 3-sigma band for all test samples. Margins of safety from the structural analysis are directly applicable to the loaded chamber for static firing loads. Based on the analysis results and the comparison of mechanical properties, no problems were predicted to occur during the firing as a result of the propellant.

Miscellaneous Data

Planned devision requests (PDR). - The following PDR's were issued against motor XJ04/0001:

PDR No.	Document	Description
259-149	83136D00132	Changed nozzle throat dimensions (ID from 5.950 to 5.816 inches)
259-150	83136D00002	Changed nozzle closure OD to fit new nozzle throat ID
259-151	83176A00002	Deletion of flight accessories (cork, paint, tunnel tabs)
259-152	83136A00042	Added shrinkage liner; changed embedment powder to HES 8666 1B; deleted hydrotest requirement; accepted 946 adhesive by specification WS 8994 rather than HS259-1-153

TABLE I

COMPARISON OF X259 MEASURED MECHANICAL PROPERTIES WITH ALLOWABLE VALUES

Properties Used in the Analysis	HI L/SN	Temperature = 77° F (298.15°K)							
		Crosshead Rate = ± 2 in./min (± 5.08 cm/min)				Crosshead Rate = ± 200 in./min (± 508 cm/min)			
		Maximum Engineering Stress, psi at 0 psig		Strain at Rupture (%)		Maximum Engineering Stress, psi at 1000 psig (6895)		Strain at Rupture (%) at 1000 psig (6895)	
		Nominal	Lower 3σ	Nominal	Lower 3σ	Nominal	Lower 3 σ	Nominal	Lower 3σ
		69(47.6)*	56(38.6)	40	31	218(150.3)	178(122.7)	53	44
Recast Dogbones	304-2	60.4 (41.6)		---		Not Tested		Not Tested	
	304-2	55.5 (38.3)		38.7					
	304-2A	57.5 (39.6)		38.7					
	304-2B	56.0 (38.6)		---					
Samples Machined from Casting Column		56.0 (38.6)		31.7		204.0 (140.7)		54.0	

Note: Maximum stress is compared in the table and deviatoric case bond stress was used for the analysis. The dogbone test samples can only measure maximum stress; however, the comparison of deviatoric stresses would give the same result as the above data.

* Values in parentheses are in Newtons/square centimeter.

PDR No.	Document	Description
259-153	83136A00042	Corrected typographical errors on PDR-259-152; added specification S83281M026 for acceptance of HES 8666-1B embedment powder
259-154	83136A00041	Changed propellant from CMDB to XLDB; mold drawing changed to 83136J00141 from ABL-259-600
259-155	83136D00133	Added PDR's 259-149 and -150 to drawing requirements
259-156	83136A00134	Added PDR 259-155; nozzle exit cone shortened; changed ASI O-ring from MS 28775-009 to 5-565-N304-7
259-157	83136A00041	Changed propellant center bore dimensions to reflect new core drawing and shrinkage liner
259-158	83136D00133	Deleted aluminum tape from nozzle outside surface

Motor components. - The major component serial numbers used in manufacture of motor XJ04/0001 are listed below:

Nomenclature	Part Number	Serial Number
Chamber	83136B00043	HPC-0213
Shrinkage liner	83159B00558 (red lined)	REC-0001
Nozzle	83136A00132 (plus PDR 259-149)	EII-1049
Igniter	83136A00110	HII-021
Forward neck liner	83136J00141-009	REC-0001
Nozzle closure	83136D00002 (plus PDR 259-150)	UPC-0004

MOTOR MANUFACTURING

Process Sequence

Manufacture of the crosslinked double base X259 demonstration motor (S/N XJ04/0001) started with a GFM hydroproofed motor chamber. Intended for static firing, the flight accessories such as exterior cork insulation, chamber bracketry, nozzle aluminum foil, paint, etc, were eliminated from the manufacturing process. The process began, therefore, with case preparation operations and proceeded through final assembly to static firing at the Bacchus Works range via the processes shown below.

Chamber preparation. - The chamber (HPC-0213) was first weighed. The forward and aft insulators were cleaned, buffed, degreased, and Epon 946 fairing was applied and allowed to cure 24 hours at room temperature.

Shrinkage liner installation was then accomplished. After being cleaned and buffed on the propellant side, and having Teflon tape applied to the dome side, the liner was bonded to the forward insulator and the fiberglass chamber wall at the forward tangent line with Epon 943 adhesive. Next the rubber casting adapter or "neck" liner was bonded to the shrinkage liner and a vacuum leak test performed. Air passage between the forward dome insulator and the dome shrinkage liner was augmented by installing strips of polypropylene netting and the Teflon tape.

Powder embedment. - A barrier coat consisting of 4 pounds (1.814 kg) of Epon 946 was sprayed into the degreased and oven-dried chamber. This coat cured for 24 hours after which an identical coat of epoxy was sprayed in and allowed to partially cure. Approximately 16 pounds (7.3 kg) of HES 8666 type powder granules were sprayed in and tumbled over the tacky surface which was then cured for 24 hours at room temperature.

Mold assembly. - In preparation for casting, the four core fins were placed in the chamber and attached to a new stronger supporting spider. The Teflon coated center core was then locked in place. The latter was modified from a standard X259 core set by welding shut the many perforations and by machining a taper to make it suitable for use with slurry casting. The completed assembly was leak tested using 13.5 psig (9.31 N/cm^2) N_2 gas pressure (Mold Assembly Drawing No. 83136J00141).

Propellant manufacture. - The propellant manufacturing process consists of ingredient preparation, binder premix, and mixing. Particle sizing of HMX is accomplished with a Jetomizer fluid energy mill. Dry ingredients are preweighed into separate mixer charging hoppers. The binder premix (acetone-dissolved nitrocellulose, nitroglycerin, PGA binder, and liquid stabilizing agents) is stripped of water and acetone and transported to the mixer in desiccators where it is then transferred to the 300 gallon (1.14 m^3) mixer bowl. The dry ingredients are slowly added to the bowl and blended before the addition of the crosslinker catalyst. Rigid controls are maintained on temperature, humidity, vacuum, and mix cycle time. Numerous laboratory analyses monitor this entire process from beginning to end.

Propellant is taken from the mix bowl and cast into dogbone molds and three OPC's (one pound charge). The dogbones are tested periodically (see below) during the cure cycle to determine when to remove the motor from heated cure and the OPC's are static fired for ballistic data.

Casting and curing. - The motor casting operation is accomplished with the assembled chamber standing in an evacuated, heated, 120° F (322° K) casting pit. Propellant is remotely cast using differential pressure to ensure a smooth flow of deaerated propellant from the sealed mix bowl to the evacuated chamber.

After casting the unit remains in the pit throughout heated cure. Hydraulic pressure (169 psig or 110.2 N/cm^2) is applied to the propellant mass through a casting reservoir and this pressure was maintained through the 14 days of heated cure and on into 3 days of cooldown.

Cooldown and core removal. - The cast and cured propellant is allowed to slowly cool down to a stress-free condition to prevent grain damage from thermal strains. The unit is then taken to the disassembly facility where the casting reservoir, with the excess propellant, is removed. The center core and the fin spider are next removed by hydraulically operated pulling fixtures, remotely controlled. The Teflon-taped fin cores are removed by hand.

Premachining X-ray and propellant machining. - The propellant mass and casebond are carefully examined by X-ray to detect voids or separations. Fin slot positions relative to the thickened areas of the chamber insulator are also confirmed. No voids or separations were detected and the insulator was determined to be properly aligned.

When motor quality has thus been established, the unit is positioned before a horizontal boring mill for cutting out the remaining casting neck and for propellant machining to grain design configuration. After machining, the loaded chamber weight is taken and the propellant weight determined.

Igniter and nozzle installation. - Flight accessories were not installed for the static firing of the XLDB demonstration motor so final assembly operations consisted of installing the igniter (HII-021) in the forward port and bolting the nozzle (EII-1049) nozzle closure assembly to the aft adapter.

The completed unit was assembled in the X259 firing harness and transported to the Bacchus Works range for static firing.

Physical Properties Data

Dogbone data. - The cure time for the XLDB propellant has not been firmly established for individual motor configurations. To determine the cure for this motor, dogbone samples from the propellant mix were tested periodically during the cure cycle. A tabulation of average pull test values (tested at 2 in./min (5.08 cm/min) and 77° F (298.2° K) is shown below:

	Days Cure	Tensile Strength (psi)	Strain at Rupture (%)	Modulus (psi)
Propellant from same mix as motor XJ04/0001 cast into dogbones	7	49.4 (34.1)*	--	198 (137)
	14	57.2 (39.4)	38.0	314 (217)
	21	66.9 (46.1)	29.5	462 (319)
	28	75.6 (52.1)	23.7	591 (407)
Dogbones machined from the propellant column taken from the forward end of motor XJ04/0001	14	56.4 (38.9)	31.7	374 (258)

*Values in parenthesis are in N/cm^2.

One pound charge data. - Three OPC motors were cast from the same mix of propellant as cast into XJ04/0001. These OPC's were static-tested to obtain propellant data. One motor failed due to a plugged nozzle, providing only two OPC's from which data was obtained. These data are used for verification of propellant burning rate.

Motor data. - The following data were obtained from the completed motor, and are compared to the X259-B4 specification data:

	Actual XJ04/0001	Nominal X259-B4
Propellant weight (lb)	2766.9 (1255.1 kg)	2565 (1163.5 kg)
Inert weight (lb)	211.1[1] (95.7 kg)	235 (106.6 kg)
Total motor weight (lb)	2978.0[1] (1350.8 kg)	2800 (1270.1 kg)

[1] Motor XJ04/0001 inert weights do not include external cork insulation, tunnel tabs, external painting (white paint, silver conductive paint, and varnish) or aluminum foil nozzle covering. The nozzle exit cone was also cut short for Bacchus Works altitude expansion. In addition, XJ04/0001 had a shrinkage liner installed in the forward end of the motor. If XJ04/0001 had been prepared for flight, 31.4 pounds (14.2 kg) of inert weight would have been added to the 211.1 (pounds (95.7 kg) to equal 242.5 pounds (110.0 kg) total motor inert weight.

Before Firing:	Actual XJ04/0001	Nominal X259-B4
Average nozzle throat dia (in.)	5.820 (14.78 cm)	5.950 (15.11 cm)
Average nozzle exit plane dia (in.)	20.251[1] (51.55 cm)	28.244 (71.74 cm)
After Firing:		
Average nozzle throat dia (in.)	6.779 (17.22 cm)	6.408 (16.28 cm)

[1] Exit cone cut short to provide a Bacchus Works altitude expansion ratio.

MOTOR STATIC FIRING

Test Plan

The X259-E6 rocket was static tested as outlined in Specific Test Plan for Static Firing X259-E6 Antares Motor S/N XJ04/0001 Loaded with High Energy Propellant, IDS Account No. 07AA023, 14 November 1973. A summary of the required test conditions is shown below:

(1) Temperature conditioning - 3 days minimum at 77 $\pm$ 5° F (298.2 $\pm$ 2.8° K)

(2) Motor installed in a modified harness, drawing 83136H00065

(3) Motor ignition initiated by one SBASI (P/N S01-10197) initiator Firing current 12 $\pm$ 2 amps.

(4) Pre- and post-throat and exit diameter measurements taken

(5) Motor quenched as soon as practical after firing

(6) Temperature and deflection measurements taken during firing

(7) Operating pressure of the igniter and motor, and motor thrust measurements are recorded

(8) Erosion measurements taken before and after motor firing

(9) Still photographs taken before and after motor firing

(10) Color motion pictures of the motor taken during firing - one high speed (400 frames/second) on the aft end, one high speed on the forward end, and two low speed (64 frames/second) on either side of the motor.

Static Firing

The rocket motor/static test fixture assembly was mounted in Bay 3 of the Bacchus Works test range. The motor was oriented horizontally in the firing harness so the aft skirt No. 1 hole (Dwg 83136B00043) was in the up 0° (0 radians) position. Looking at the aft end of the motor and measuring clockwise, the propellant slots were located at 60° (1.05 rad), 120° (2.09 rad), 240° (4.19 rad), and 300° (5.24 rad). To protect for reflective heating of the thermocouples, the aft dome was covered with zinc chromate putty and crinkled aluminum foil. A thermocouple was inserted through a hole in the styrofoam nozzle closure to measure grain temperature. The motor was temperature-conditioned in the test bay at 77 $\pm$ 5° F (298.2 $\pm$ 2.8°K) for five days prior to static test. The motor was fired at approximately 2:00 p.m. on 20 February 1974.

Test Results

Ballistic evaluation. - The motor did not perform as predicted. All of the propellant was consumed but because the nozzle failed, the performance was less than planned. Except for the nozzle, the chamber aft adapter, and the fiberglass area adjacent to the aft adapter, the postfired condition of the motor was typical of that found on other successful X259 motors. (See Figures 1 through 5.)

The chamber, except as noted, was uncharred. The igniter was intact and attached to the forward closure, and the insulator char was within the expected range considering the actual environment. In addition, the condition of the forward shrinkage liner, used for the first time, was as expected. A shrinkage liner tail of approximately nine inches (23 cm) attached to the motor forward tangent line remained in the motor.

The nozzle was scattered widely over the static test range from immediately aft of the motor to about 250 yards (229 m) away (throat/retainer ring assembly). The nozzle had fragmented into innumerable pieces. From the movies and physical examination of the nozzle parts, the nozzle evidently came apart gradually throughout most, if not all, of the motor operating time.

Table II shows the sequence of events noted during the motor firing. The first visual observation of a failure was a glow appearing on the nozzle surface approximately 1 to 3 inches (2.5-7.6 cm) aft of the attach ring at about 90° (1.57 rad) which then opened to form a pencil of flame. (See Figures 6 and 7.) Two more jets of flame appeared, one about 1-1/4 inches (3.1 cm) above, and another about 1-1/4 inches (3.1 cm) below the first. The flame then progressed around the nozzle from about 0° (0 rad) to about 190° (3.32 rad). The entire sequence from the appearance of the first red glow, starting at about 12 seconds, to the propagated flame was complete in about 2.3 seconds. The motor then continued burning essentially unchanged for 13.2 seconds at which time the major portion of the exit cone ejected. About one second (29.4 seconds) later a section of the retainer ring ejected (see Figures 8 and 9) dropping the pressure to 70 psi (48.3 N/cm^2). Calculations of the throat area required to maintain 70 psi (48.3 N/cm^2) motor pressure show that the remaining throat/retainer ring assembly did not leave the motor until about 38 seconds after ignition. Figure 10 shows the total throat area change with respect to time. This throat area includes leakage through the retainer ring vent holes.

Thrust and pressure versus time curves are presented in Figures 11 through 14 and are compared with predictions. Table III shows a comparison of predicted performance values.

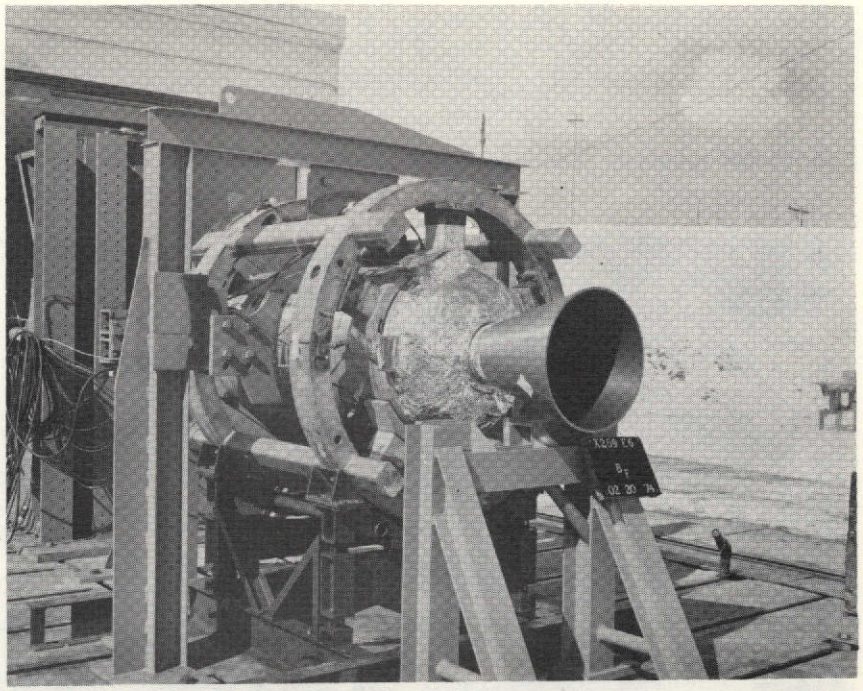

Figure 1. Motor Before Firing, South-East View, 270° (4.71 rad) at Left, XJ04/0001

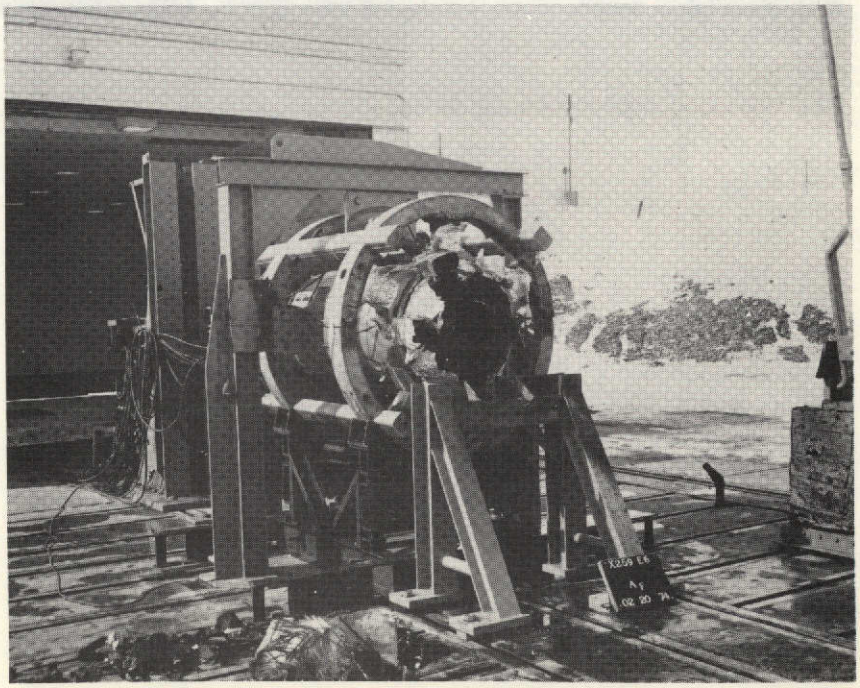

Figure 2. Motor After Firing, South-East View, XJ04/0001

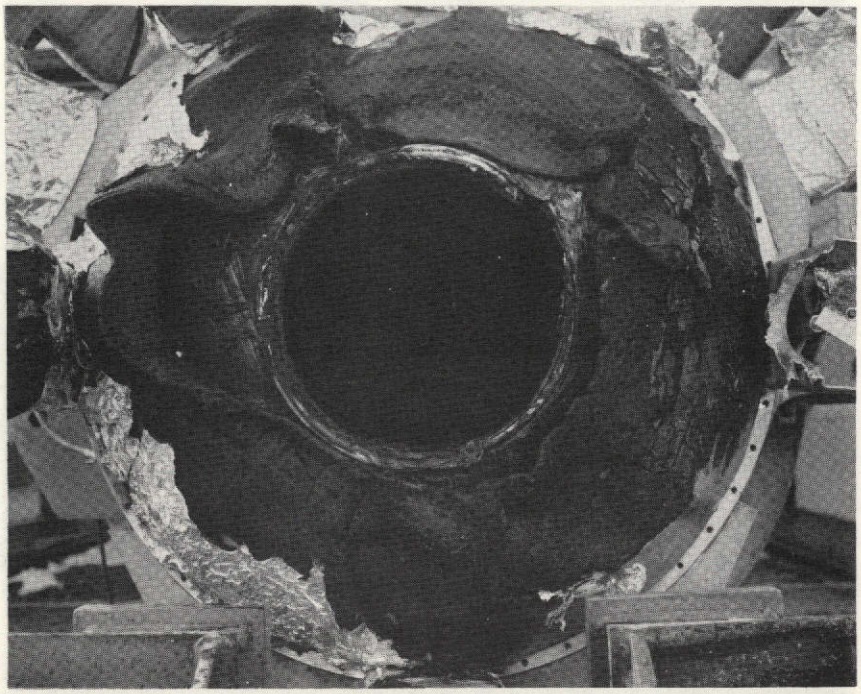

Figure 3. Close-up of the Motor Aft End After Firing, XJ04/0001

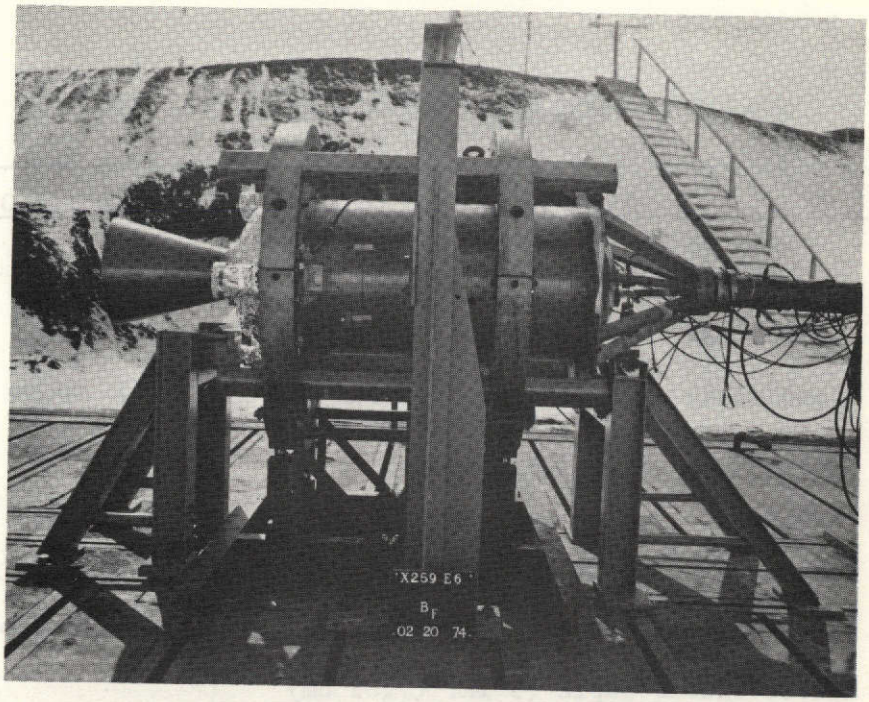

Figure 4. Motor Before Firing, North View, 90° (3.32 rad) on Near Side, XJ04/0001

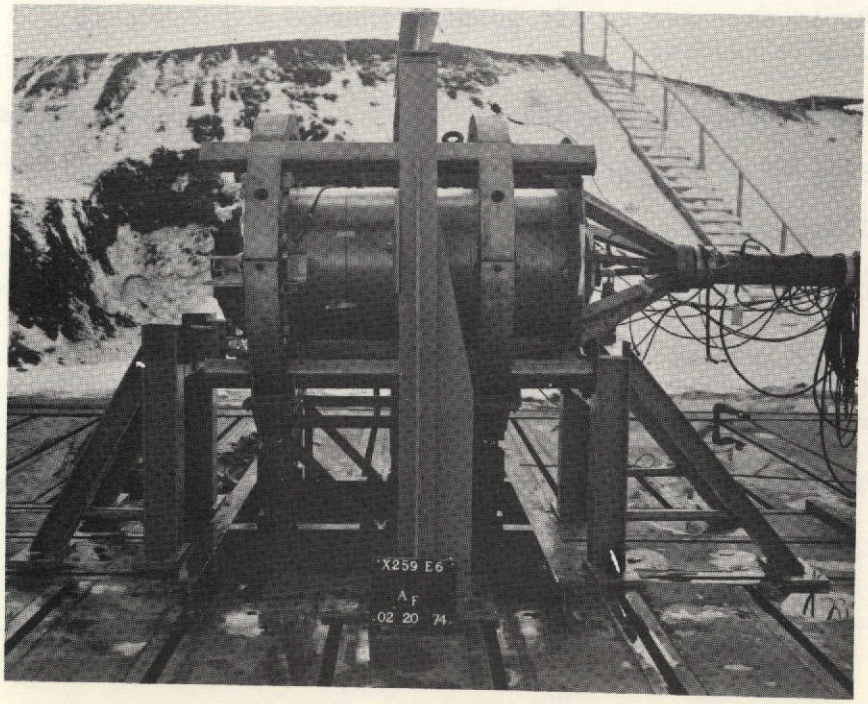

Figure 5. Motor After Firing, North View, XJ04/0001

TABLE II

XJ04/0001 FIRING SEQUENCE OF EVENTS

Time (sec)	Event	Noted On
0.103	Time to 90% of ignition pressure	Pressure-time Curve
12.0	First flame visible on exit cone O.D.	Movie Film
14.3	Flame flashed around nozzle O.D.	Movie Film
14.7	Disturbance in exhaust plume	Movie Film
	Oscillations in thrust record	Thrust-time Curve
	Change in slope of F/P Curve	Calculated Data
	Perturbation in nozzle thermocouples	3 Thermocouples
16.6	Nozzle thermocouple (3 in. (7.62 cm) aft of adapter) lost	T NOZ-9
27.5	Exit cone ejected	Movie Film Thrust-time Curve F/P Curve
28.6	Rapid increase in aft adapter thermocouple reading	T NOZ-11
29.4	Rapid pressure decrease	Pressure-time Curve
	Segment of "retainer ring" ejected	Movie Film
	Thermocouple on nozzle lost	T NOZ-12
35.0	Deluge started	Movie Film
38.0	Large, red-glowing items ejected (probably the remaining throat/retainer ring assembly)	Movie Film Visual Observation
39.0	Chamber pressure returns to ambient	Pressure-time Curve
53.0	Quench started	Movie Film

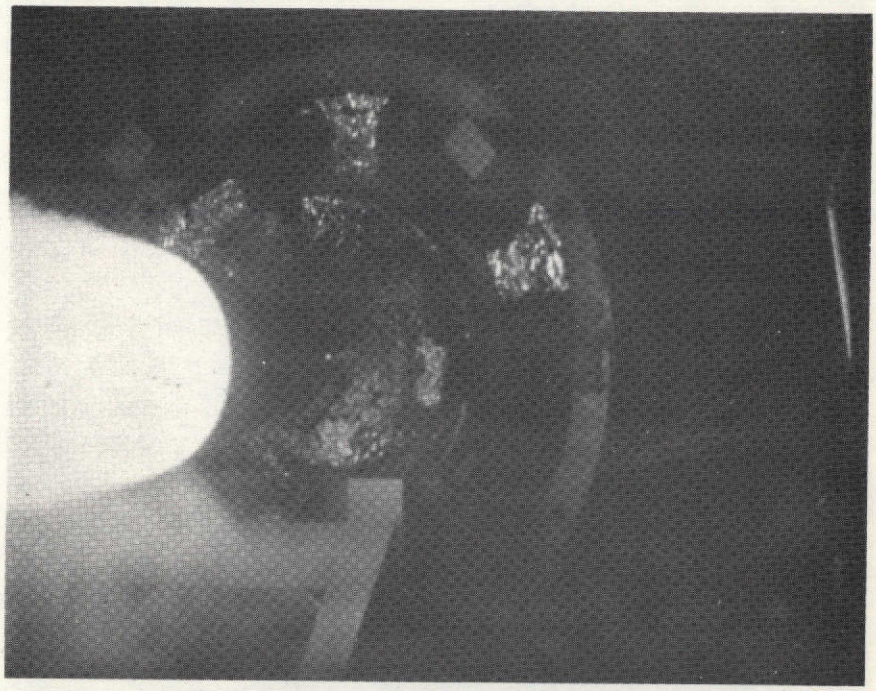

Figure 6. First Appearance of Flame on Nozzle. Taken from 400 Frames per Second Movie Film Located North-East of Motor

Figure 7. Appearance of Flame 0.4 Seconds After Figure 6 View. Taken From 400 Frames per Second Movie Film Located North-East of Motor

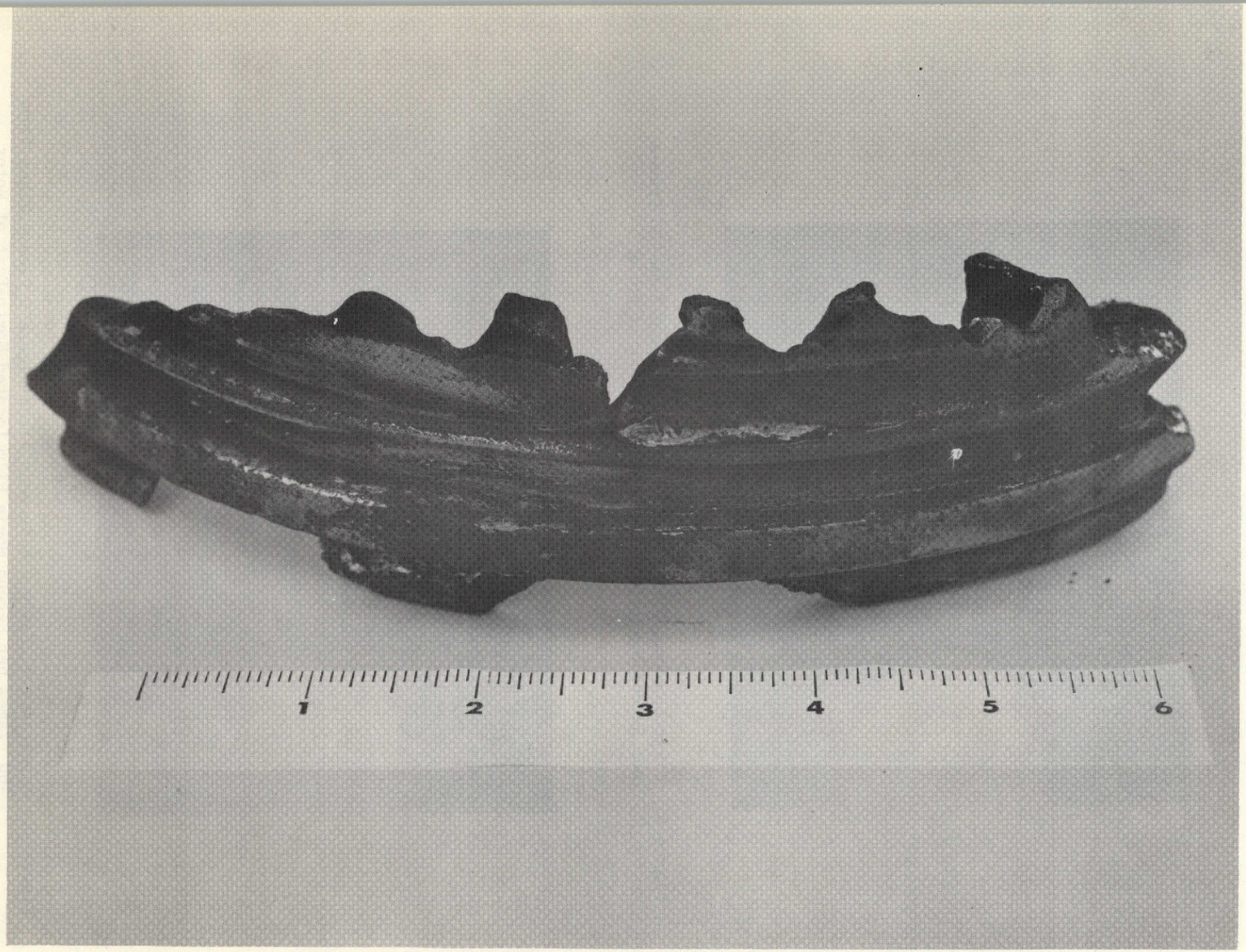

Figure 8. Retainer Ring Section (Showing O-ring Groove) Ejected From Motor at 29.4 Seconds

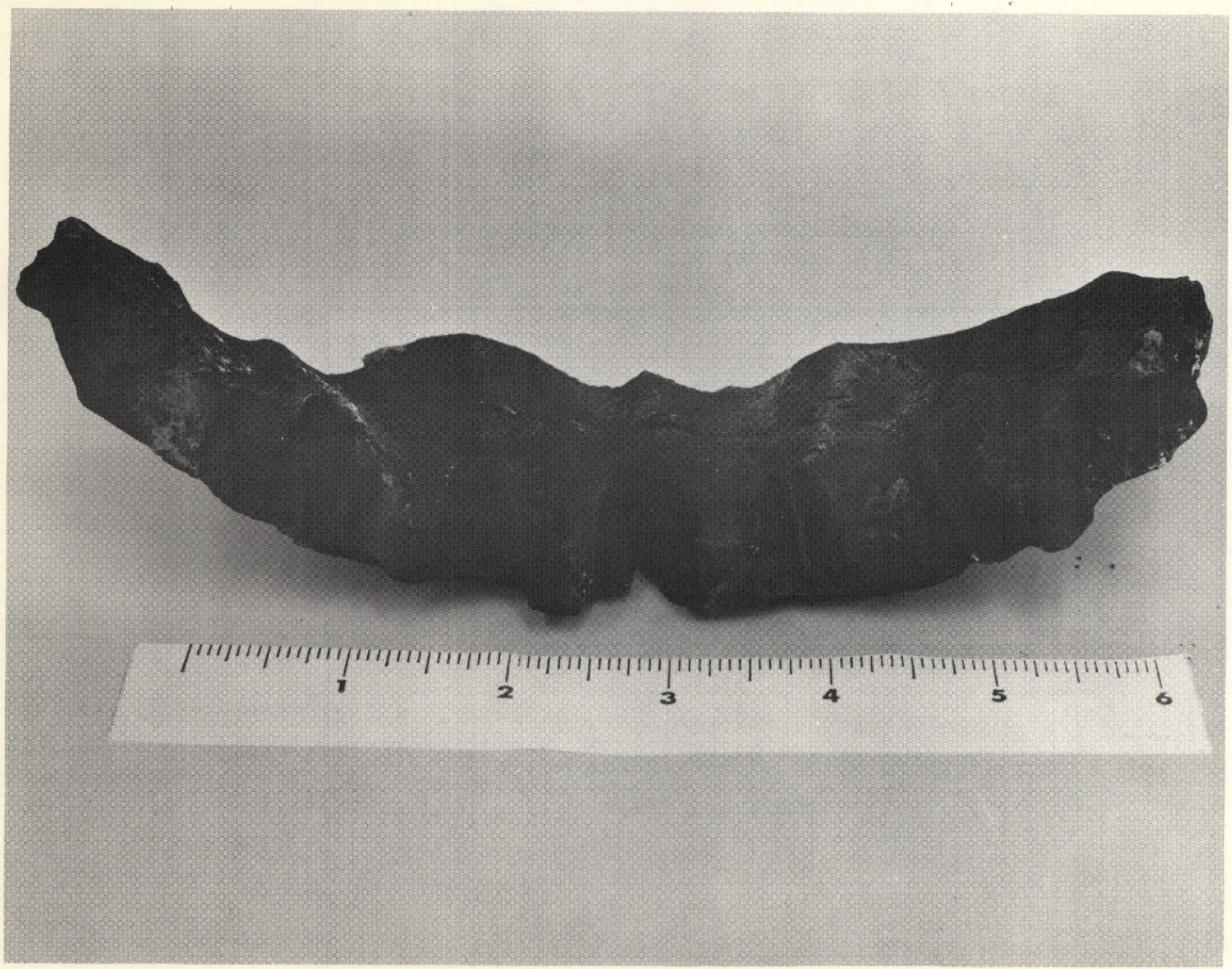

Figure 9. Retainer Ring Section (Showing Inside Diameter View) Ejected From Motor at 29.4 Seconds

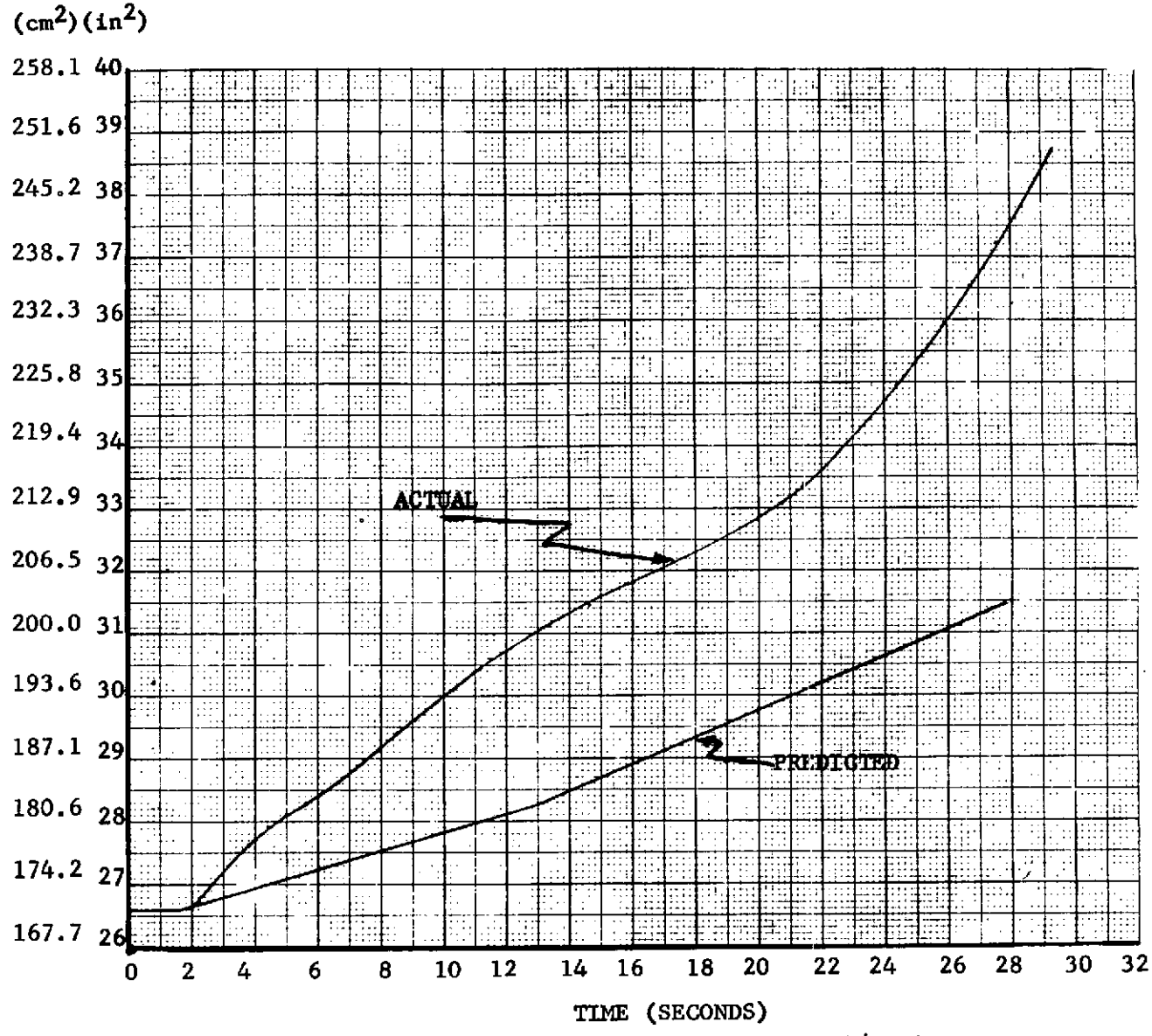

Figure 10 - Throat Area vs Time of Motor XJ04/0001

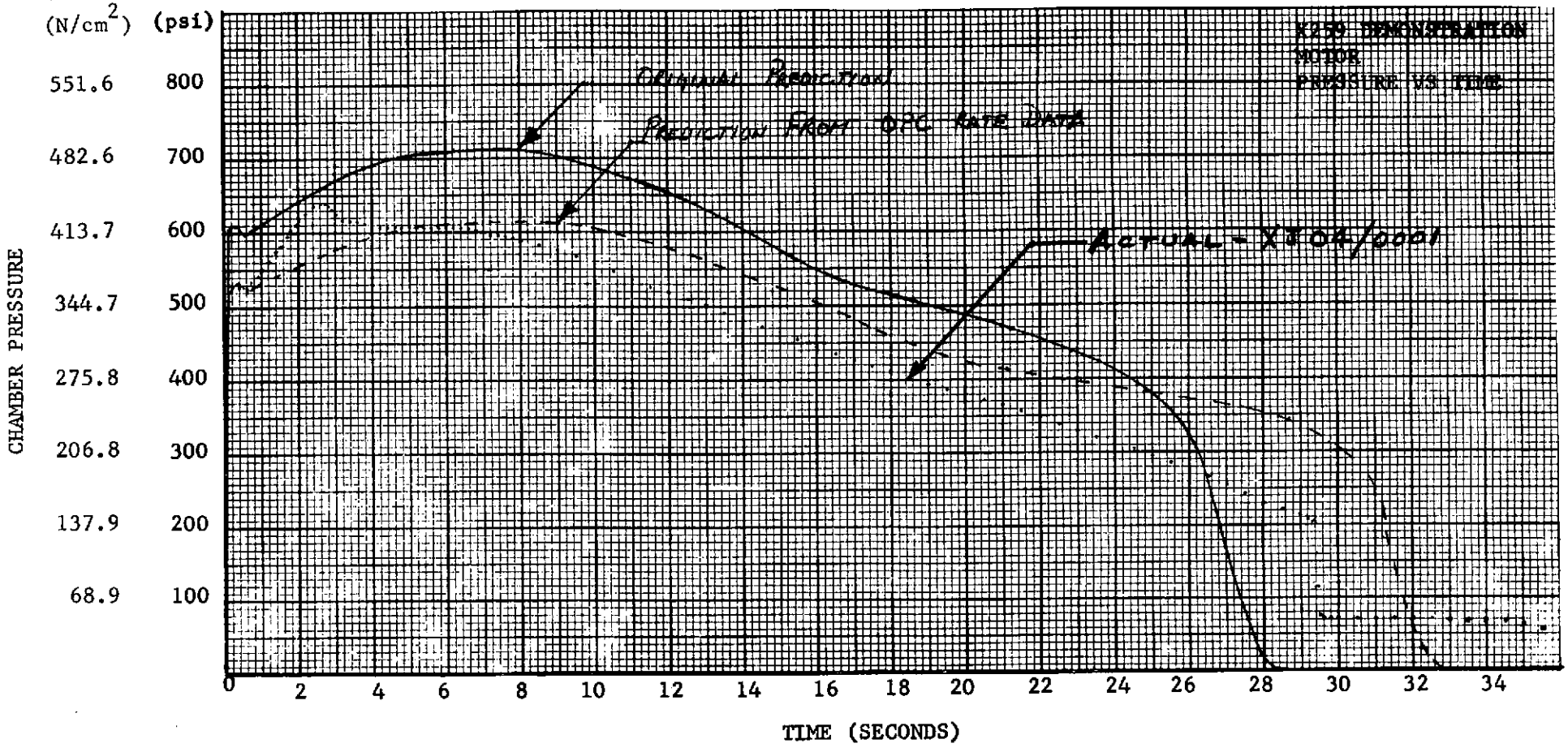

Figure 11 - Replotted Motor Pressure Curve and Predicted Curves for Comparison

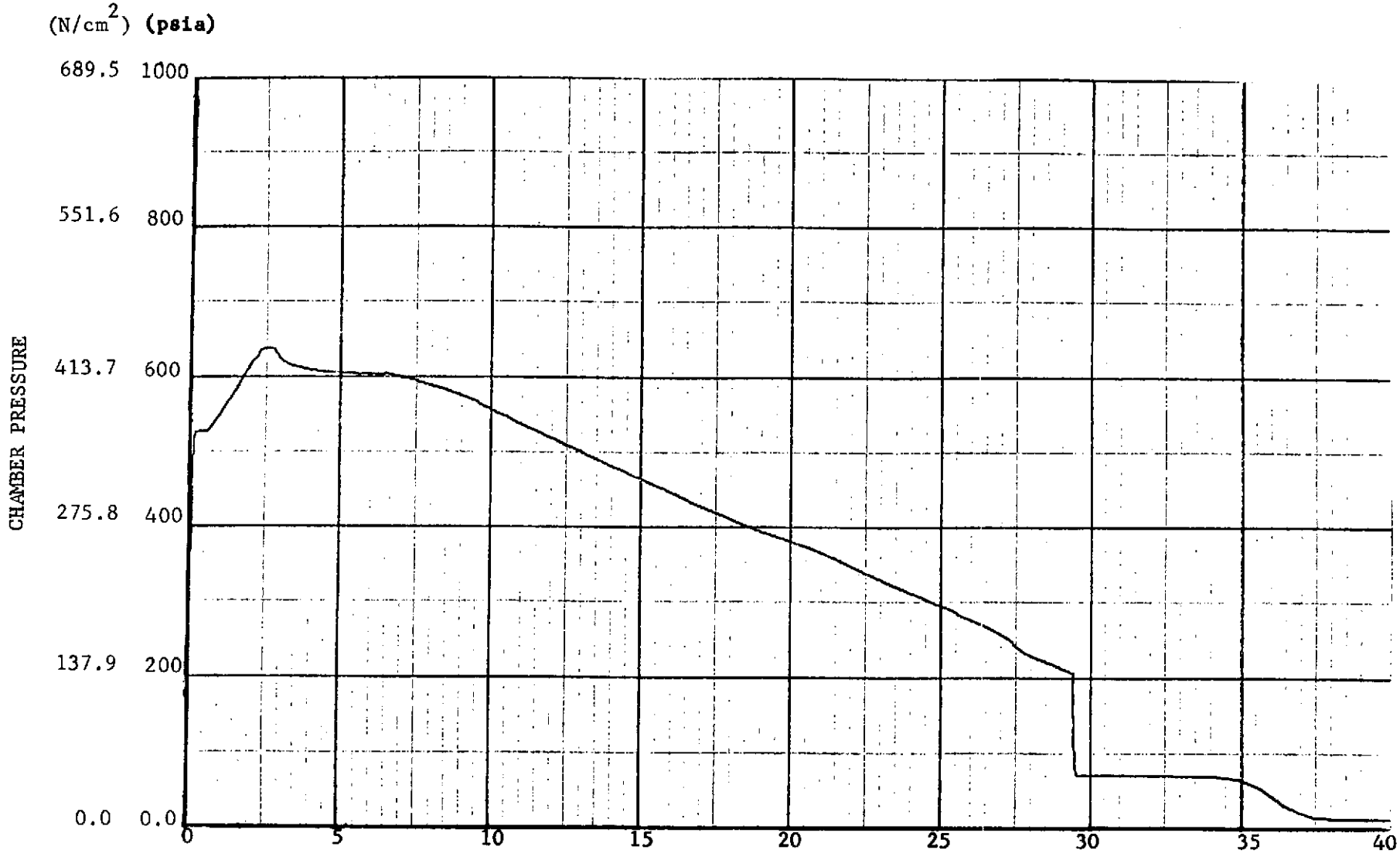

Figure 12 - Computer Plot of Motor Pressure Versus Time

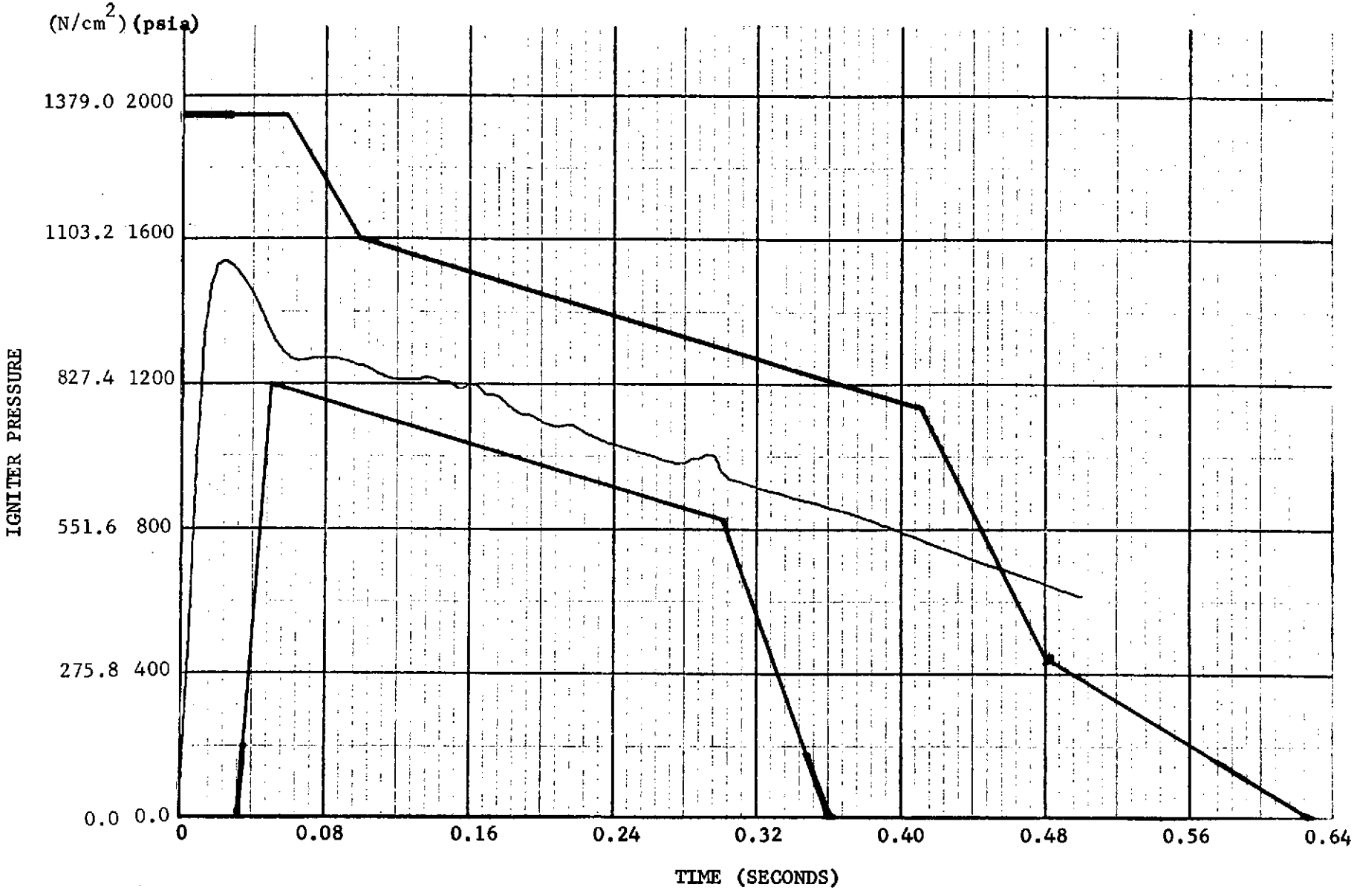

Figure 13 - Computer Plot of Igniter Pressure Showing Specification (HS259-2-170) Limits

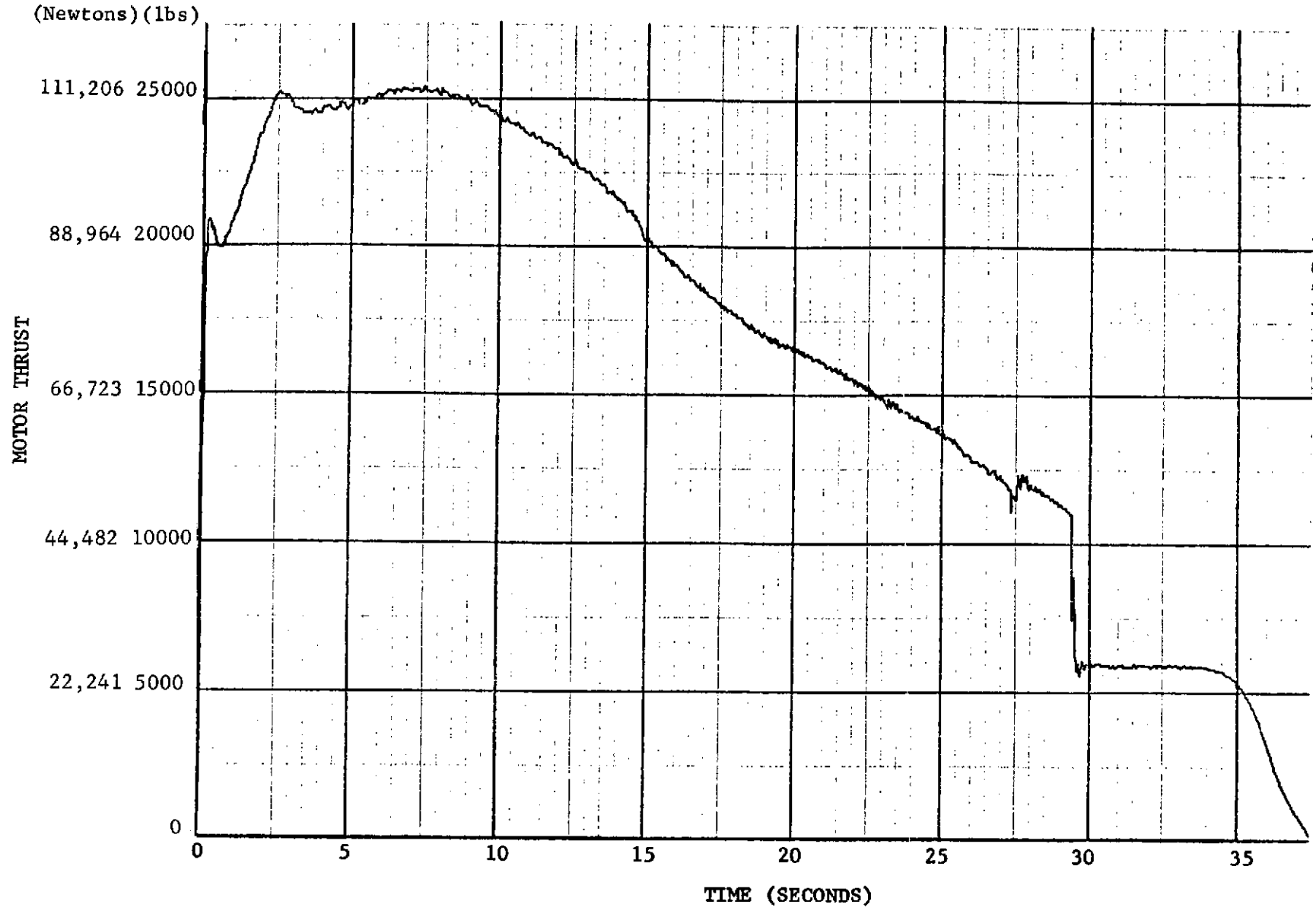

Figure 14 - Computer Plot of Actual Motor Thrust.

TABLE III

COMPARISON OF PREDICTED VS ACTUAL VALUES

	X259-B4	Predicted X259 Demo (1)	Repredicted X259 Demo (2)	Actual (XJ04/0001) X259 Demo
Max Pressure (psia)	607 (418.5 N/cm^2)	750 (517.1 N/cm^2)	614 (423.3 N/cm^2)	639 (440.6 N/cm^2)
Average Pressure (psia)	515 (355.0 N/cm^2)	570 (393.0 N/cm^2)	463 (319 N/cm^2)	455 (3) (314 N/cm^2) 364 (4) (251 N/cm^2)
Burn Time (seconds)	26.5	27.6	33.1	29.4 38
Propellant Weight (lb)	2568 (1165 kg)	2746 (1246 kg)	2746 (1246 kg)	2766 (1255 kg)
Initial Throat (dia) (in.)	5.950 (15.11 cm)	5.760 (14.63 cm)	5.760 (14.63 cm)	5.820 (14.78 cm)

(1) Predicted in September 1973. Based on rate and performance data from forty pound charge data.

(2) Predicted in February 1974. Based on one pound charge data of OPC's cast from actual XJ04/0001 propellant lot.

(3) Average pressure at burntime of 29.4 seconds

(4) Average pressure at burntime of 38 seconds

Analysis of Failure

The first indication of failure, from the motion pictures, was a flame appearing aft of the nozzle attach ring. The flame was observed to be almost perpendicular to the nozzle surface. To explain this and the resultant nozzle failure, three postulated mechanisms are presented below.

The first mechanism, the most likely of the three, consists of spalling of a piece of the nozzle throat followed by loss of a piece of exit cone liner. The second postulation assumes leakage through the retainer ring vent holes. The third possible failure mode theorizes that a piece of the exit cone liner ejected on ignition.

Possible failure mechanism No. 1 (ejection of a throat insert section): The most likely mechanism of the nozzle failure is shown in Figure 15 and described below.

An aft section of the throat, at 90° (1.57 rad), was ejected from the motor. The direction of the wrap is 45° (0.785 rad), facing upstream. An examination of the throat after firing shows this section of the throat missing and it is evident that localized plies of throat wrap were coming off during the firing. (See Figures 16 and 17.) This, because of the succeeding events, must have occurred within the initial two seconds of motor operation.

The ejection of the throat material resulted in two events. One was a more rapid erosion of the throat in the region of the missing material as shown in Figure 18, 90° (1.57 rad) being located on the north side of the motor, Figure 19. This high erosion was reflected in the lower-than-predicted pressure noted in the pressure versus time curve. The second effect was the spalling of a section, or sections, of the graphite/phenolic exit cone liner.

Expulsion of the exit cone liner exposed the asbestos/phenolic back-up material. Assuming a reasonable 20 mils/sec (0.51 mm/sec) erosion rate of the asbestos/phenolic due to the abnormal gas flow across this material, the first burnthrough would occur at 12 seconds. The locations of the three evenly spaced burnthrough locations correspond to the spacing of the longitudinal grooves machined in the outside surface of the asbestos/phenolic. The distinctness of these burnthrough spots could have been agitated by the sine wave machining of the graphite-asbestos interface and the slight overdrilling of the liner vent holes (which have the proper spacing, but it appears unlikely that the holes would be in line with the grooves).

The ejection of the throat aft section and resultant flow across the exposed surface eventually would reveal the retainer ring 0.062 inch (0.16 cm) diameter vent holes. As these vent holes are opened, gas would start to flow through them. The velocity through these holes would initially be in the range of 1800 ft/sec (549 m/sec). From the erosion data of Figure 20, this started at about 16 seconds. The erosion opened up a leakage area of about 7 $in.^2$ (45.15 cm^2) as shown in Figure 21.

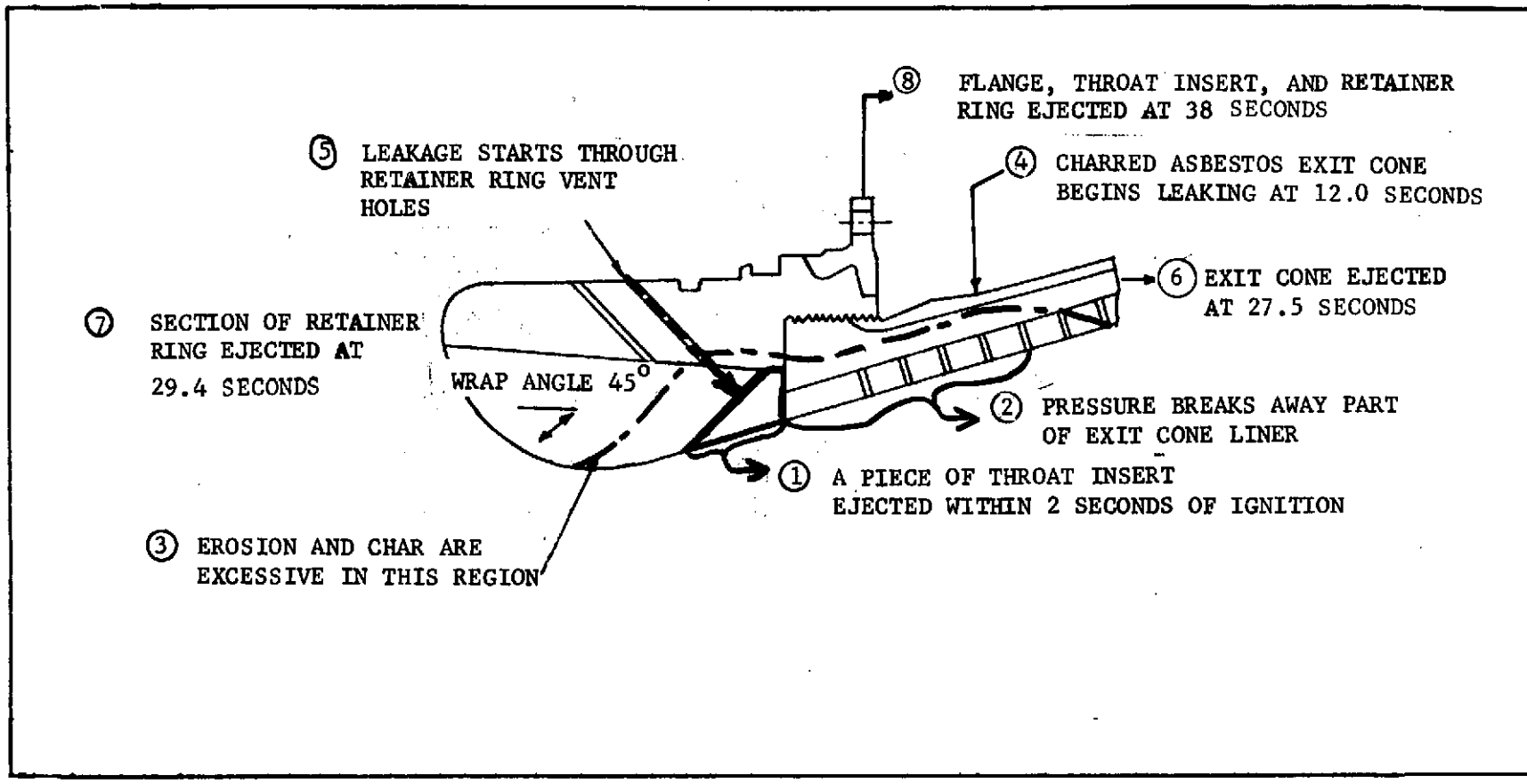

Figure 15 - Nozzle Failure Sequence of Events, Possible Failure Mechanism No. 1

Figure 16. Nozzle Throat/Retainer Ring Assembly, 180° (3.14 rad) View

Figure 17. Nozzle Throat/Retainer Ring Assembly, 270° (4.71 rad) View

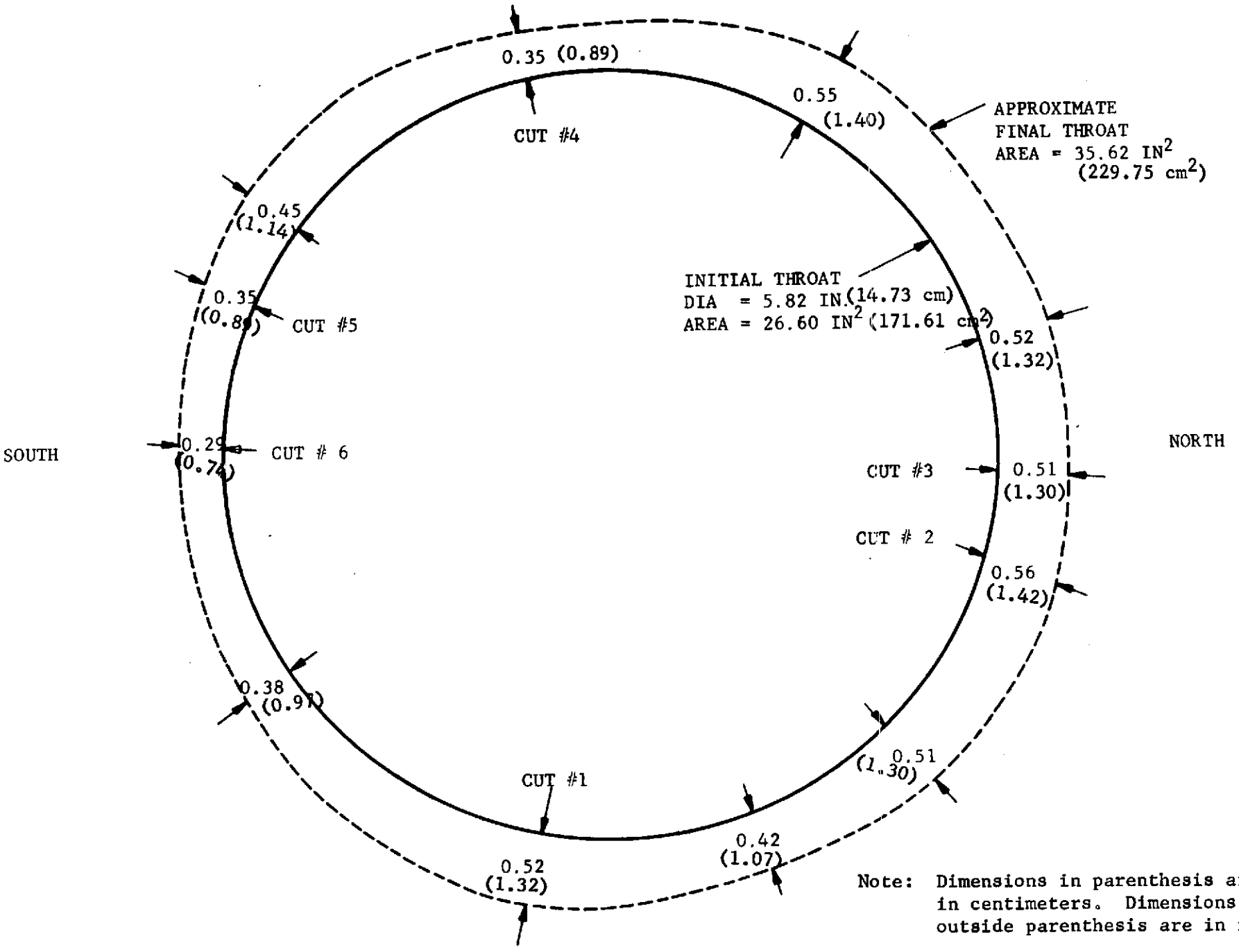

Figure 18 - Comparison of Inital and Final Nozzle Throats, Motor XJ04/0001

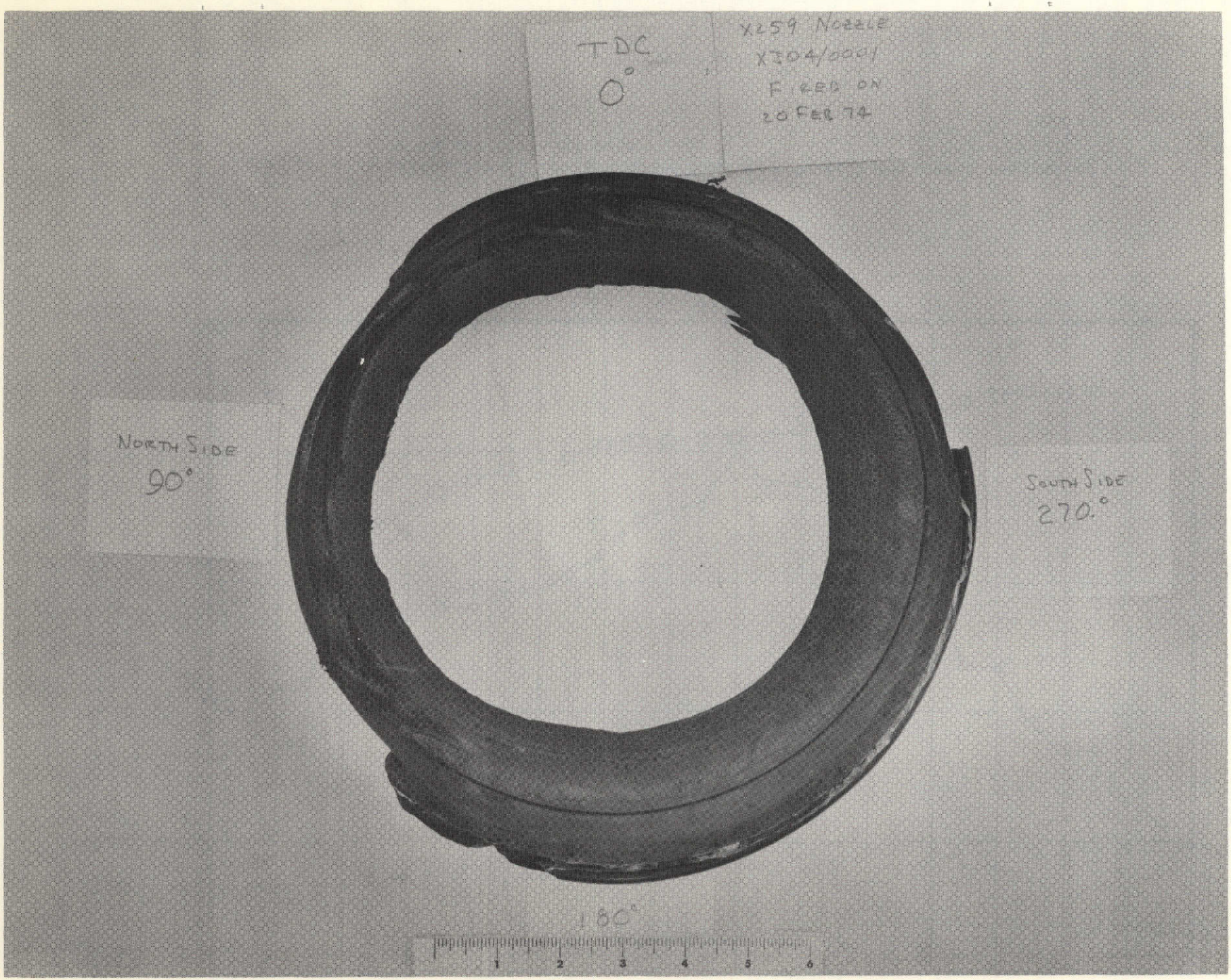

Figure 19. View of Throat After Firing

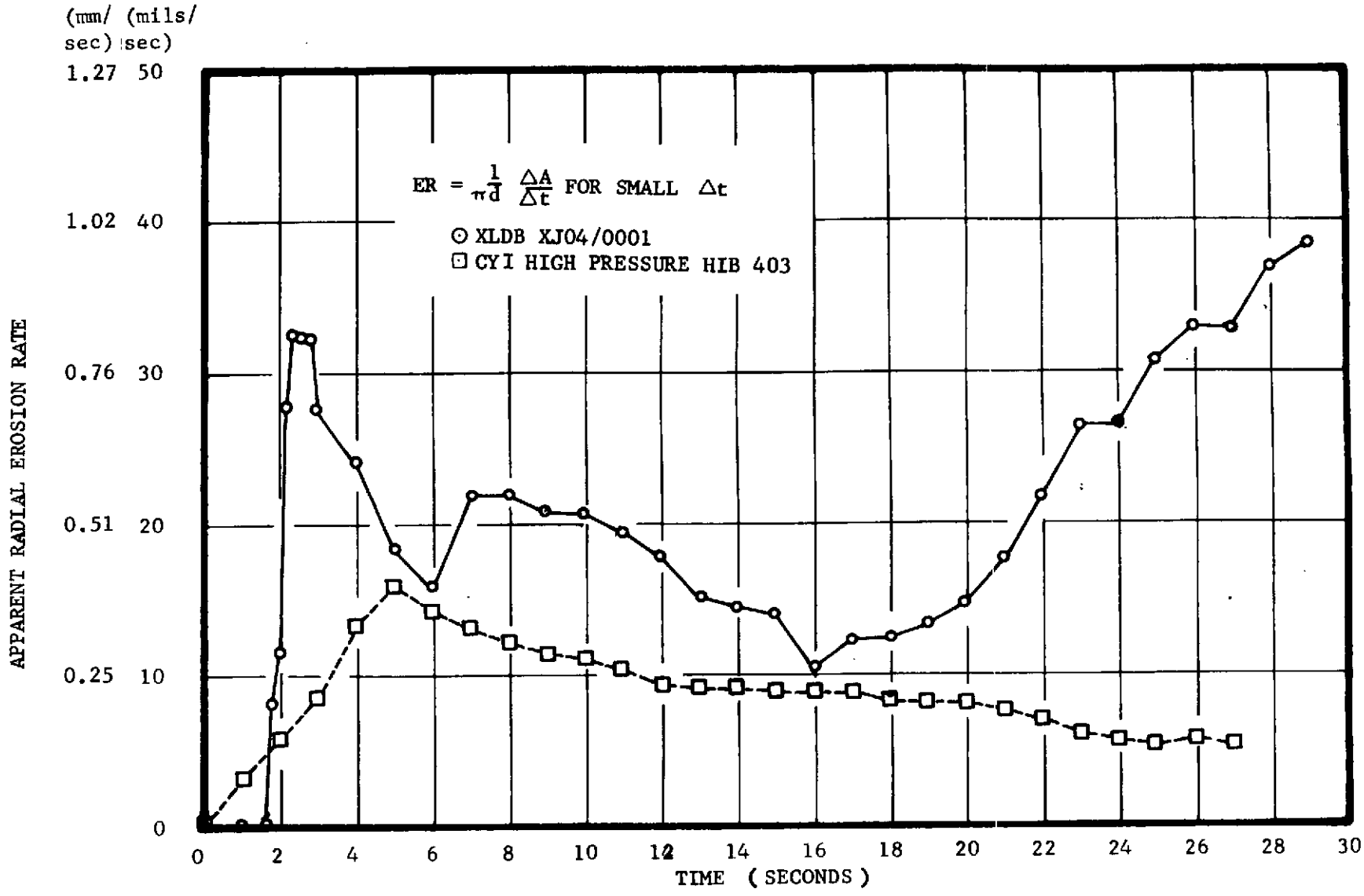

Figure 20 - Apparent Throat Erosion Rates Measured in X259 Firings - Determined from Thrust/Pressure Data

Figure 21. Assembly of Retainer Ring Section and Nozzle Throat/Retainer Ring Assembly Showing Side Leakage Area

At 29.4 seconds, a rapid pressure drop occurred and a change in the plume shape was observed. The pressure drop from 200 psi (137.9 N/cm^2) to 70 psi (48.3 N/cm^2) corresponds to opening an additional area equal to the cross-sectional area of the retainer ring section expelled from the motor. (See Figure 8.) The side retainer ring vent area plus the throat area equals the area required to maintain a 70 psi (48.3 N/cm^2) motor pressure.

The retainer ring section was picked up 150 yards (137.16 m) northeast of the motor (the nozzle end of the motor faced east). The remaining throat/retaining ring assembly (Figure 16) was probably expelled at 38 seconds. As noted above, the motor pressure corresponds to ejection late in the firing. In addition, red streaks were seen in the movie film and a large red glowing object was seen by observers in the air at about 38 seconds. This assembly was found 250 yards (228.6 m) east-northeast from the motor.

The reason for the initial release and ejection of nozzle throat aft section is not known. Possible explanations include: (1) The XLDB propellant exhaust environment may be more severe than that found with conventional X259 CYI propellant (two successes with CYI and this nozzle throat design, HIB-403 and HPC-209), (2) material imperfections in the graphite/phenolic throat, or (3) a combination of these two items.

Possible failure mechanism No. 2 (retainer ring vent holes leakage): Figure 22 summarized the following sequence of events related below.

A leak starts in the retainer ring vent holes on ignition and follows the bondline to the exit cone liner and returns into the exhaust stream.

At 12.0 seconds the gas leakage through the vent hole/bondline path has degraded the adhesive at the retainer ring threads sufficiently to allow leakage directly through the threads or through the porous fiberglass overwrap. The three pencil-shaped areas of flame, described in postulation 1, correspond to the circumferential hole spacing in the retainer ring, or the spacing in the longitudinal grooves in the exit cone liner.

Gas leakage continues to erode the retainer ring vent holes. (See Figure 21.) The chamber pressure drops off as the vent holes grow. The retainer ring erosion ranges from 0.40 inch (1.02 cm) to 0.70 inch (1.78 cm) radially from the original vent holes. This implies erosion rates of 13.5 mils/sec (0.34 mm/sec) to 23.7 mils/sec (0.75 mm/sec) for a 29.4 second burn time, at which time a rapid pressure drop occurs. (See postulation 1, above.) These erosion rates seem too small for the exhaust eroding ability of the XLDB propellant used in motor XJ04/0001 when eroding a throat of RPD-150 asbestos/phenolic; therefore, leakage probably occurred over a shorter time period than 29.4 seconds.

The throat insert continues to be eroded from the backside aft of the retainer ring vent holes until no insert material remained in the area of the venting gases.

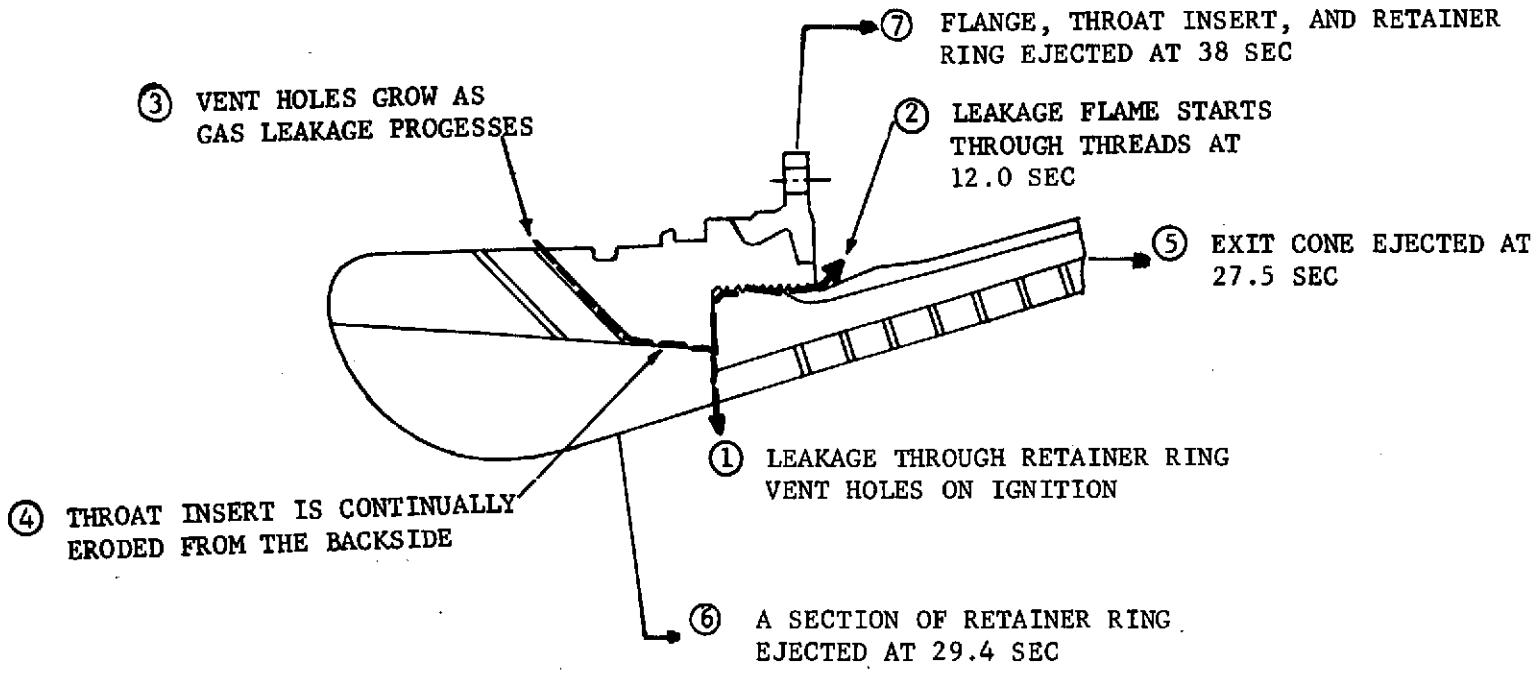

Figure 22. Nozzle Failure Sequence of Events, Possible Failure Mechanism No. 2

Postulation 1, above, describes succeeding events.

There are some unanswered questions that need to be resolved before accepting the above failure mode. These are:

(1) The nozzle was pressure-tested and no leakage was observed.

(2) The three fingers of flame were observed to be aft of the nozzle attach ring by 1 to 3 inches (2.5 to 7.6 cm), not at the threaded interface.

(3) If there was a gas leakage path through the threads, leakage would begin at ignition or not at all. Adhesive in the threads should be sufficient to prevent gas leakage.

(4) The retainer ring vent holes are assumed to erode for 29.4 seconds. The total erosion around the vent holes is too low for this exposure time.

Possible failure mechanism No. 3 (ejection of a piece of exit cone liner): This failure mechanism is essentially the same as that of postulation 1, above, except for the initial event, ejection of a piece of the exit cone liner on motor ignition. (See Figure 23.)

Upon ignition, a piece of graphite/phenolic exit cone liner is ejected, exposing the asbestos exit-cone insulation.

Assuming a reasonable 20 mils/sec (0.51 mm/sec) erosion rate of the asbestos/phenolic due to the abnormal gas flow across this material, the first burnthrough would occur at 12 seconds. The locations of the three evenly spaced burnthrough locations correspond to the spacing of the longitudinal grooves machined in the outside surface of the asbestos/phenolic. The distinctness of these burnthrough spots could have been agitated by the sine wave machining of the graphite-asbestos interface and the slight overdrilling of the liner vent holes (which have the proper spacing but it is unlikely that they would be in line with the grooves).

Heat from the gases degrade the throat insert-to-retainer ring bond in the area of the missing exit cone liner. The degraded adhesive provides a leak path for the retainer ring vent holes. The leakage through these vent holes results in additional throat area. As the vent holes are opened, gas would start to flow through them. The velocity through the holes would initially be in the range of 1800 ft/sec (549 m/sec). From the erosion data of Figure 20, this started at about 16 seconds. This erosion opened up a leakage area of about 7 $in.^2$ (45.15 cm^2) as shown in Figure 21.

Postulation 1, above, describes succeeding events.

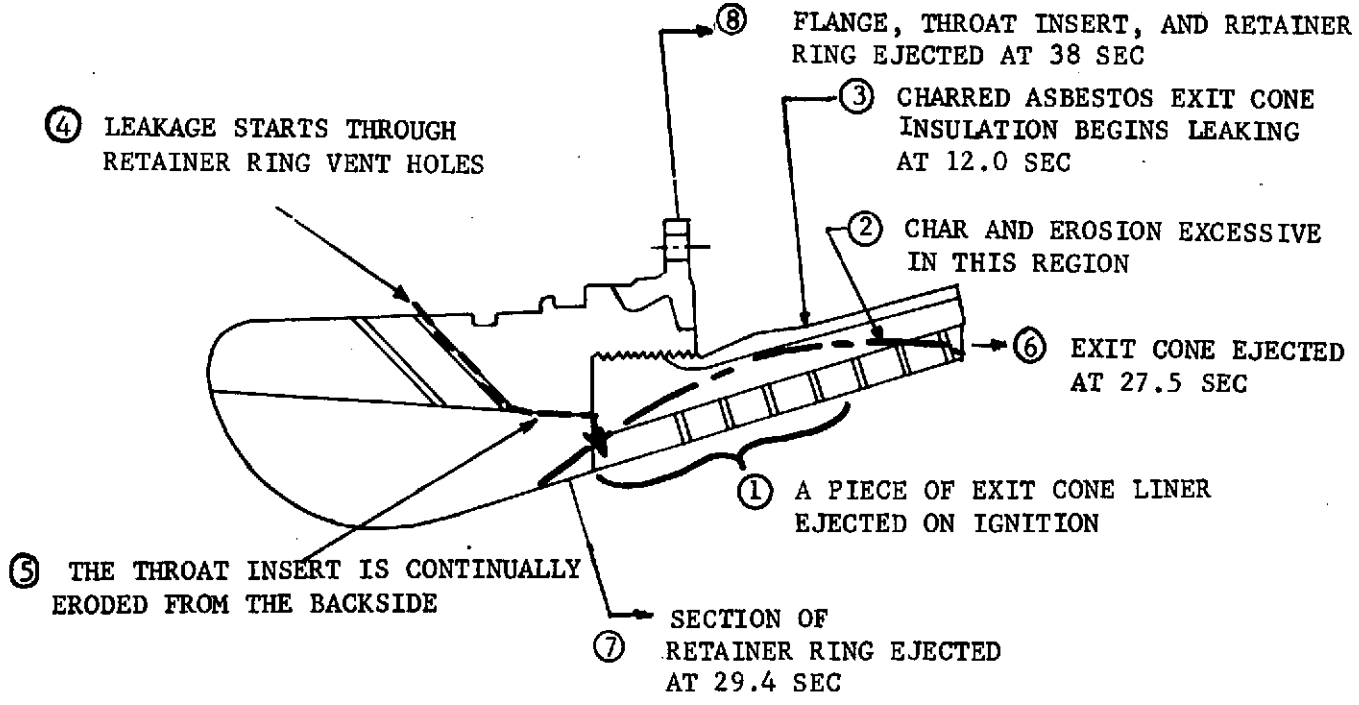

Figure 23. Nozzle Failure Sequence of Event, Possible Failure Mechanism No. 3

One unanswered question remains. There is no apparent reason, either from manufacturing, inspection, or from the slightly more severe environment of the XLDB propellant (over CYI propellant), for a piece of the exit cone liner to be ejected.

Insulator. - Insulator char depths were the same or less than in motors of comparable burn time. These char depths were not excessive considering the nozzle failure which caused a longer-than-expected exposure and an unknown flow environment. The only anomaly noted was the three percent greater char depths in line with the slots near 90 degrees (where the first pressure leak was observed in the nozzle). Tables IV and V show the motor char data and Figure 24 identifies the measurement locations.

Thermocouple Data. - Eleven thermocouples were attached to the chamber and nozzle, as shown in Figure 25. The thermocouple locations correspond to those of X259-B4 motor HIB-403 that was static fired at AEDC on 31 August 1973.

The thermocouple plots are shown in Figures 26 through 36. These plots were made by the computer and include system noise. All thermocouples recorded valid data throughout the firing except for TNOZ-9, TNOZ-11, and TNOZ-12 which lost data at 16.6 seconds, 31.3 seconds, and 29.4 seconds, respectively.

Deflectometer Measurements. - The test plan required three skirt-to-skirt deflection measurements separated by 120 degrees. Because of interference with the test harness, the deflectometers were relocated and one additional deflectometer was added to locate them at:

Deflectometer	Location
LP-301	180° (3.14 rad)
LP-302	90° (1.57 rad)
LP-303	270° (4.71 rad)
LP-304	25° (0.44 rad)

The elongation measurements of LP-301, -302, and -303 compare favorably with those generated in X259 chambers HPC-0202, -0211, -0214, -0215, and -0216 hydrotest data. The five hydrotest chamber deflections ranged from 0.2 to 0.4 inch (0.5 to 1 cm) at 640 psi (441 N/cm^2) chamber pressure. Deflectometer number LP-304, for an unknown reason, indicated maximum deflection of only 0.084 inch (0.21 cm). Deflection data are shown in Figures 37 through 40.

TABLE IV

X259 MOTOR DATA SUMMARY

Motor	Propellant		Average Pressure (psia)	Motor Action Time (sec)	Initial Motor Temperature (^{o}F)	Postfire Quench
	Name	Weight (lbm)				
Low Pressure Predicted	CYI-75 (CMDB)	2568.0	343.	33.4	N/A	N/A
YL-01/0003	CYI-75 (CMDB)	2568.3	306.	37.5	40	40 sec after burnout
YJ-01/0016	CYI-75 (CMDB)	2567.8	343.	33.4	80	5 sec after burnout
HPC-18	CYI-75 (CMDB)	2564.5	367.	31.081	100	No quench
High Pressure Predicted	CYI-75 (CMDB)	2568.0	650.	26.0	N/A	N/A
XJ03/0003 (HIB-403)	CYI-75 (CMDB)	2560.5	515.	26.5	70	No quench
XLDB Predicted	XLDB1	2746.0	573.	27.5	N/A	N/A
XJ04/0001	XLDB1	2766.9	454. 379.	29.4* 36.46**	70	53 sec after ignition

*Throat was lost

**To 30 Psi

TABLE IV - Concluded

X259 MOTOR DATA SUMMARY
(Repeated in International Units)

Motor	Propellant Name	Propellant Weight (kg)	Average Pressure N/cm^2	Motor Action Time (sec)	Initial Motor Temp. ($^{\circ}$ K)	Post-fire Quench
Low Pressure Predicted	CYI-75 (CMDB)	1164.84	236	33.4	N/A	N/A
YL01/0003	CYI-75 (CMDB)	1164.98	211	37.5	277.6	40 sec after quench
YL01/0016	CYI-75 (CMDB)	1164.75	236	33.4	299.8	5 sec after burnout
HPC-18	CYI-75 (CMDB)	1163.26	253	31.081	627.4	No quench
High Pressure Predicted	CYI-75 (CMDB)	1164.84	448	26.0	N/A	N/A
XJ03/0003 (HIB-403)	CYI-75 (CMDB)	1161.44	355	26.5	294.3	No quench
XLDB Predicted	XLDB1	1245.59	395	27.5	N/A	N/A
XJ04/0001	XLDB1	1255.07	313 261	29.4* 36.46**	294.3	53 sec after ignition

*Throat was lost
** To 20 N/cm^2

TABLE V

X259 MOTORS COMPARATIVE INTERNAL INSULATOR CHAR DEPTHS

Station[3]	Nominal Initial Insulator Thickness (inch)[4]	Average[1] Char Depth[2] (inch) for Various X259 Motors								
		CYI-75 CMDB Propellant						XLDB1 Propellant		
		Low Pressure				High Pressure		Predicted		Measured
		Predicted	Measured			Predicted	Measured	Normal Burn Time	XJ-04/0001 Burn Time	
			YL-01/0003	YJ-01/0016	HPC-18[5]		XJ-03/0003			XJ-04/0001
F1	0.290	0.026	--- ---	--- ---	0.055	---	--- ---	0.020	---	--- ---
F2	0.210	0.015	--- ---	--- ---	0.080	---	--- ---	0.012	---	--- ---
A	0.185	0.014	0.006 (0.000/0.014)	0.001 (0.000/0.002)	0.070	0.025	0.0 (0.000/0.000)	0.011	---	0.0 (0.000/0.000)
B	0.114	0.005	0.0 (0.000/0.000)	0.0 (0.000/0.000)	0.030	0.008	0.0 (0.000/0.000)	0.004	---	0.0 (0.000/0.000)
C	0.088	0.003	0.0 (0.000/0.000)	0.0 (0.000/0.000)	0.020	0.003	0.0 (0.000/0.000)	0.003	---	0.0 (0.000/0.000)
GG	0.645	0.256	0.295 (0.268/0.337)	0.209 (0.164/0.255)	0.270	0.188	0.183 (0.175/0.190)	0.177	0.235	0.296 (0.288/0.308)
DD	0.588	0.241	0.249 (0.2Z9/0.268)	0.261 (0.258/0.267)	0.330	0.192	0.193 (0.192/0.194)	0.169	0.224	0.283 (0.267/0.300)
Z	0.490	0.224	0.200 (0.165/0.244)	0.202 (0.185/0.214)	0.280	0.195	0.148 (0.142/0.154)	0.152	0.201	0.265 (0.242/0.297)
V	0.405	0.178	0.144 (0.124/0.171)	0.172 (0.163/0.185)	0.220	---	0.141 (0.132/0.149)	0.138	0.183	0.197 (0.190/0.200)
R	0.310	0.188	0.126 (0.107/0.153)	0.128 (0.107/0.144)	0.170	---	0.096 (0.094/0.098)	0.137	0.182	0.169 (0.142/0.191)
N	0.310	0.183	0.116 (0.107/0.121)	0.130 (0.120/0.144)	0.210	---	0.072 (0.067/0.077)	0.134	0.178	0.165 (0.157/0.180)
J	0.240	0.105	0.076 (0.062/0.086)	0.073 (0.065/0.080)	0.140	---	0.058 (0.050/0.066)	0.081	0.107	0.104 (0.087/0.120)
G	0.150	0.047	0.024 (0.013/0.046)	0.040 (0.027/0.061)	0.080	---	0.009 (0.008/0.010)	0.037	0.049	0.071 (0.058/0.079)

1. Minimum and maximum measured char depth all in parenthesis (0.200/0.300).

2. Char depth defined as shown:

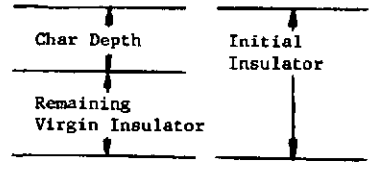

3. See Figure 22- Aft dome locations are inline with propellant slots.

4. Tolerance is $^{+0.020"}_{-0.010"}$

5. Only average char depth is listed in report.

TABLE V - Concluded

X259 MOTORS COMPARATIVE INTERNAL INSULATOR CHAR DEPTHS
(Repeated in International Units)

Station[3]	Nominal Initial Insulator Thickness (cm)[4]	Average[1] Char Depth[2] (cm) for Various X259 Motors								
		CYI-75 CMDB Propellant						XLDB1 Propellant		
		Low Pressure				High Pressure		Predicted		Measured
		Predicted	Measured			Predicted	Measured	Normal Burn Time	XJ-04/0001 Burn Time	XJ-04/0001
			YL-01-0003	YJ-01/0016	HPC-18[5]		XJ-03/0003			
F1	0.737	0.066	-- --	-- --	0.140	--	-- --	0.051	--	-- --
F2	0.533	0.038	-- --	-- --	0.203	--	-- --	0.030	--	-- --
A	0.470	0.036	0.015 (0.000/0.036)	0.003 (0.000/0.005)	0.178	0.064	0.0 (0.000/0.000)	0.028	--	0.0 (0.000/0.000)
B	0.290	0.013	0.0 (0.000/0.000)	0.0 (0.000/0.000)	0.076	0.020	0.0 (0.000/0.000)	0.010	--	0.0 (0.000/0.000)
C	0.224	0.008	0.0 (0.000/0.000)	0.0 (0.000/0.000)	0.051	0.008	0.0 (0.000/0.000)	0.008	--	0.0 (0.000/0.000)
GG	1.638	0.650	0.749 (0.718/0.856)	0.531 (0.417/0.648)	0.686	0.478	0.465 (0.445/0.483)	0.450	0.597	0.752 (0.732/0.782)
DD	1.494	0.612	0.632 (0.582/0.681)	0.663 (0.655/0.678)	0.838	0.488	0.490 (0.488/0.493)	0.169	0.569	0.719 (0.678/0.762)
Z	1.245	0.569	0.508 (0.491/0.620)	0.513 (0.470/0.544)	0.711	0.495	0.376 (0.361/0.391	0.386	0.511	0.673 (0.615/0.754)
V	1.029	0.452	0.366 (0.315/0.434)	0.323 (0.414/0.470)	0.559	--	0.358 (0.335/0.378)	0.351	0.465	0.500 (0.483/0.508)
R	0.787	0.478	0.320 (0.272/0.389)	0.325 (0.272/0.366)	0.432	--	0.244 (0.239/0.249)	0.348	0.462	0.429 (0.361/0.485)
N	0.787	0.465	0.295 (0.272/0.307)	0.330 (0.305/0.366)	0.533	--	0.183 (0.170/0.196)	0.340	0.452	0.419 (0.399/0.457)
J	0.610	0.267	0.193 (0.157/0.218)	0.185 (0.165/0.203)	0.356	--	0.147 (0.127/0.168)	0.206	0.272	0.264 (0.221/0.305)
G	0.381	0.119	0.061 (0.033/0.117)	0.102 (0.069/0.155)	0.203	--	0.023 (0.020/0.025)	0.094	0.124	0.180 (0.147/0.201)

1. Minimum and maximum measured char depth all in parenthesis (0.200/0.300)

2. Char depth defined as shown:

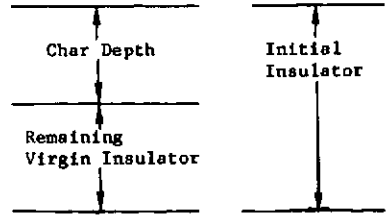

3. See Figure 22 - Aft dome locations are inline with propellant slots.

4. Tolerance is $^{+0.051}_{-0.025}$

5. Only average char depth is listed in report.

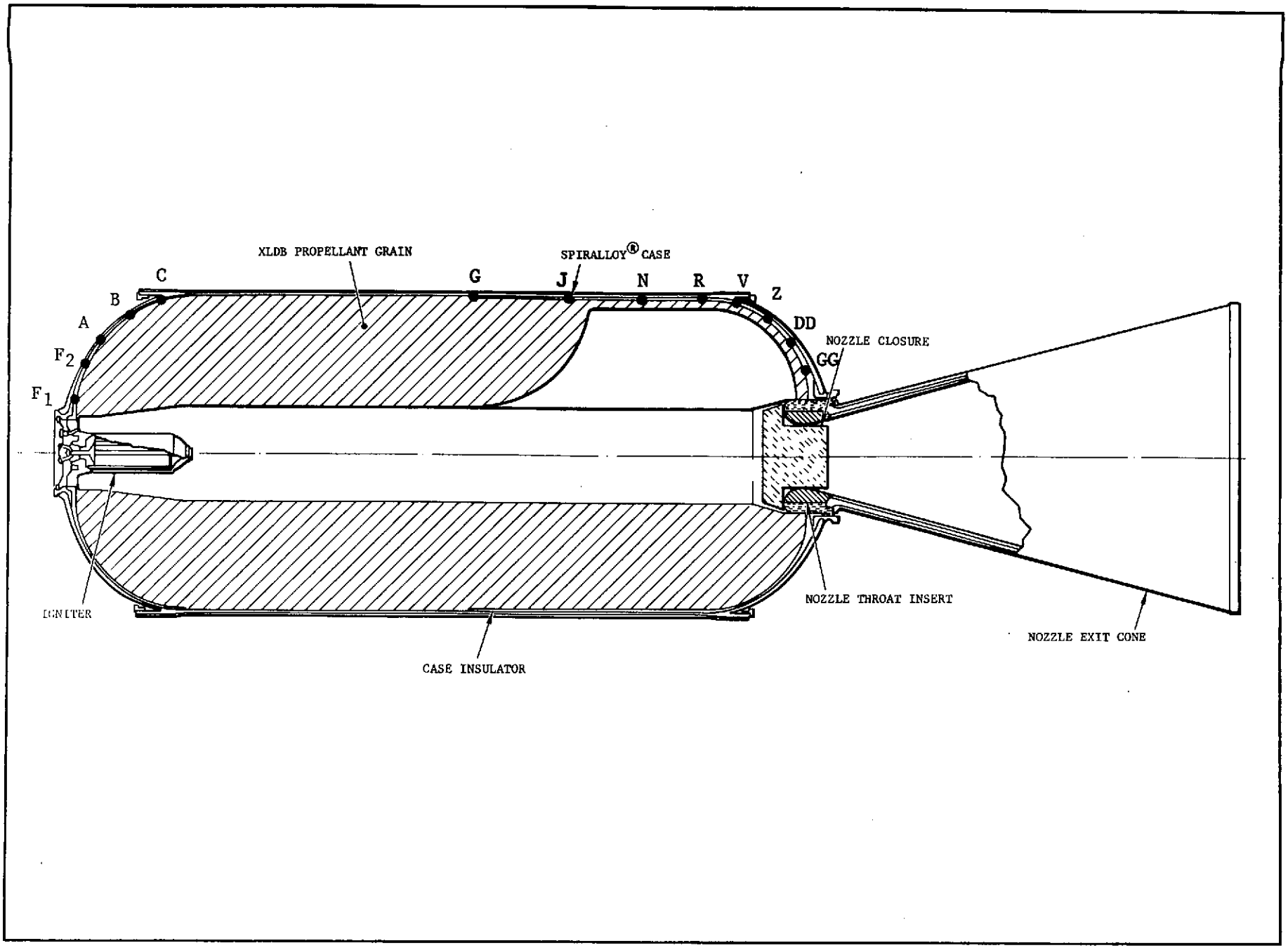

Figure 24 - Internal Insulator Analysis Station Locations

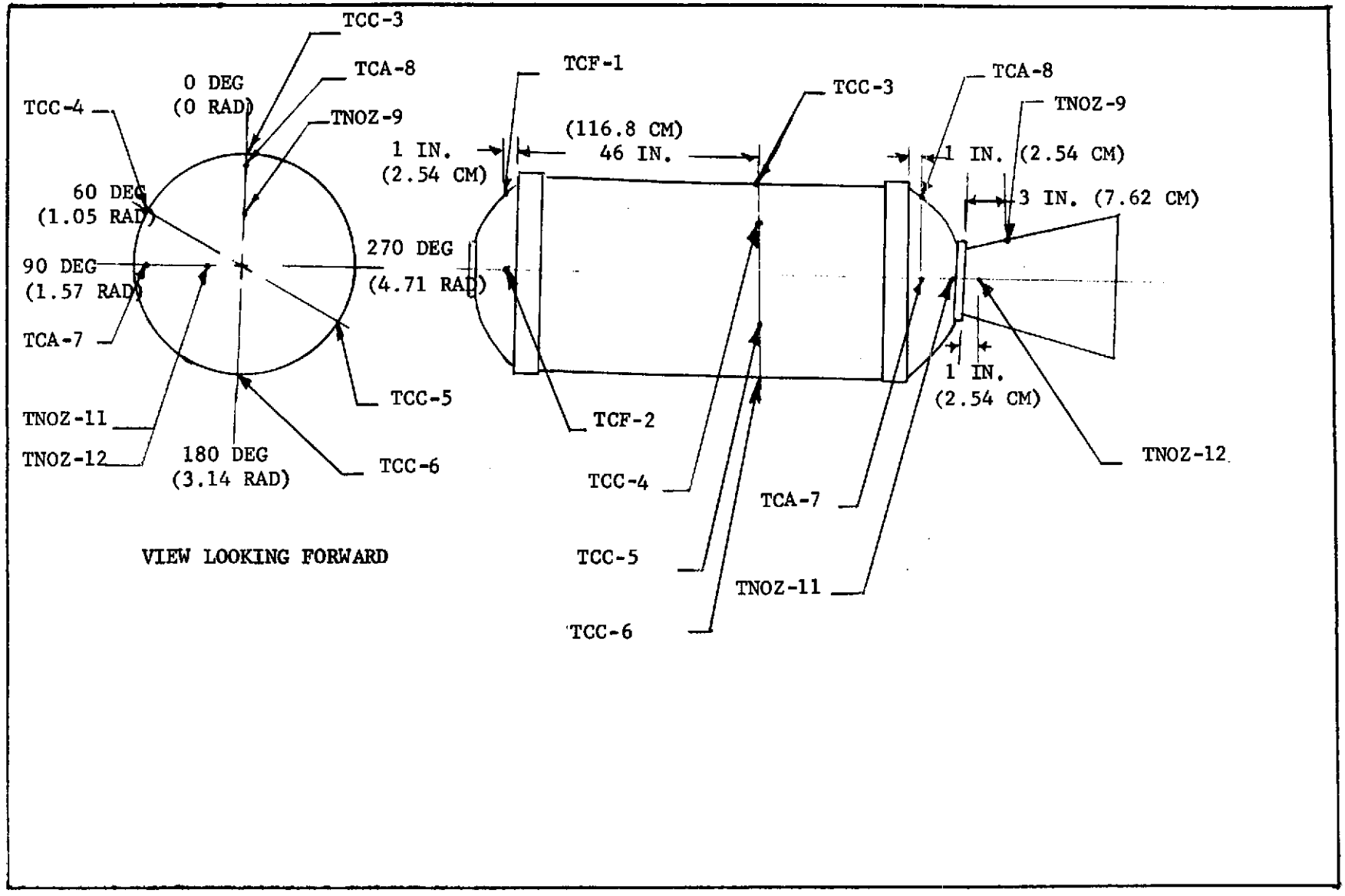

Figure 25. Thermocouple Locations

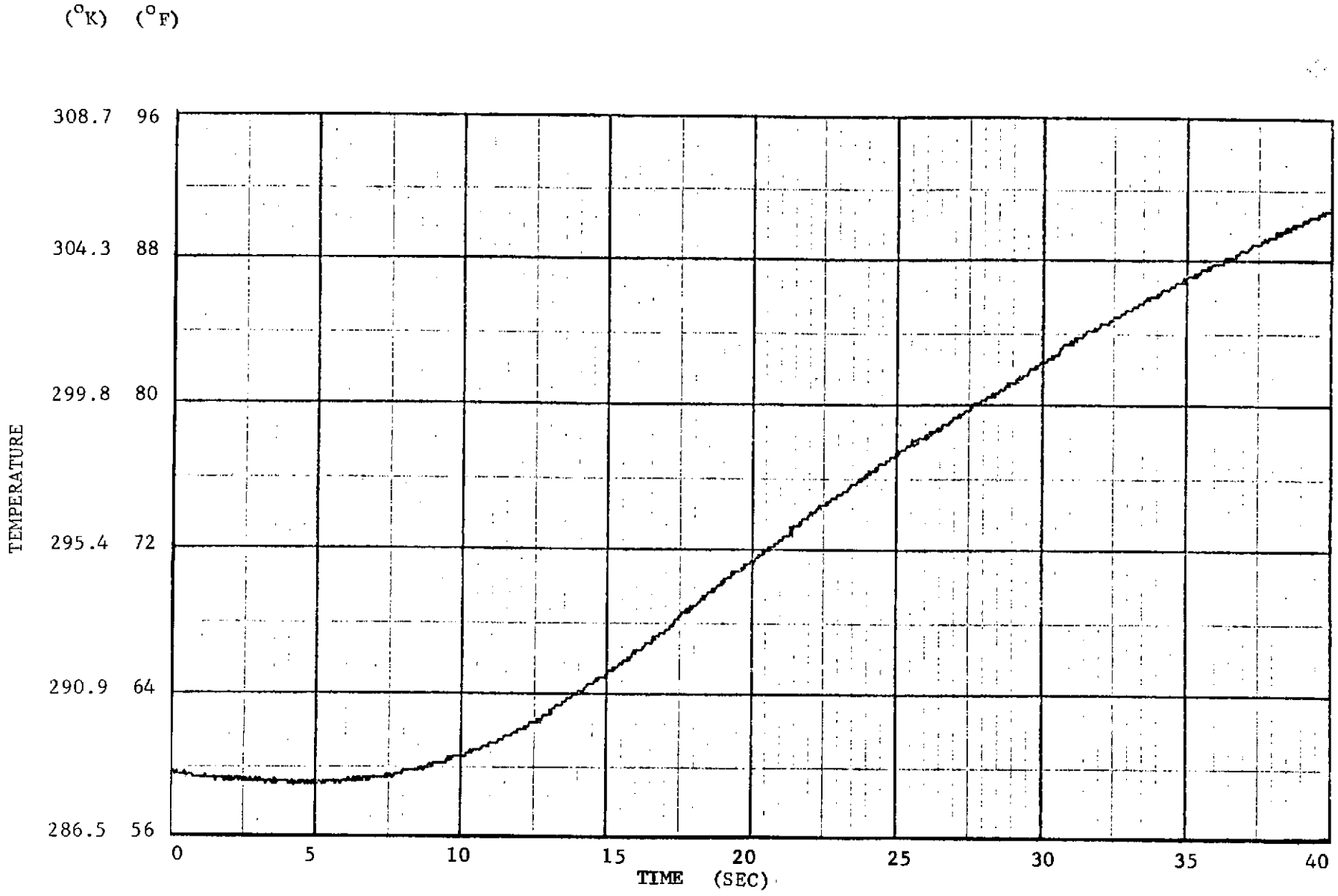

Figure 26. Temperature Versus Time Computer Plot of Thermocouples TCF-1, XJ04/0001

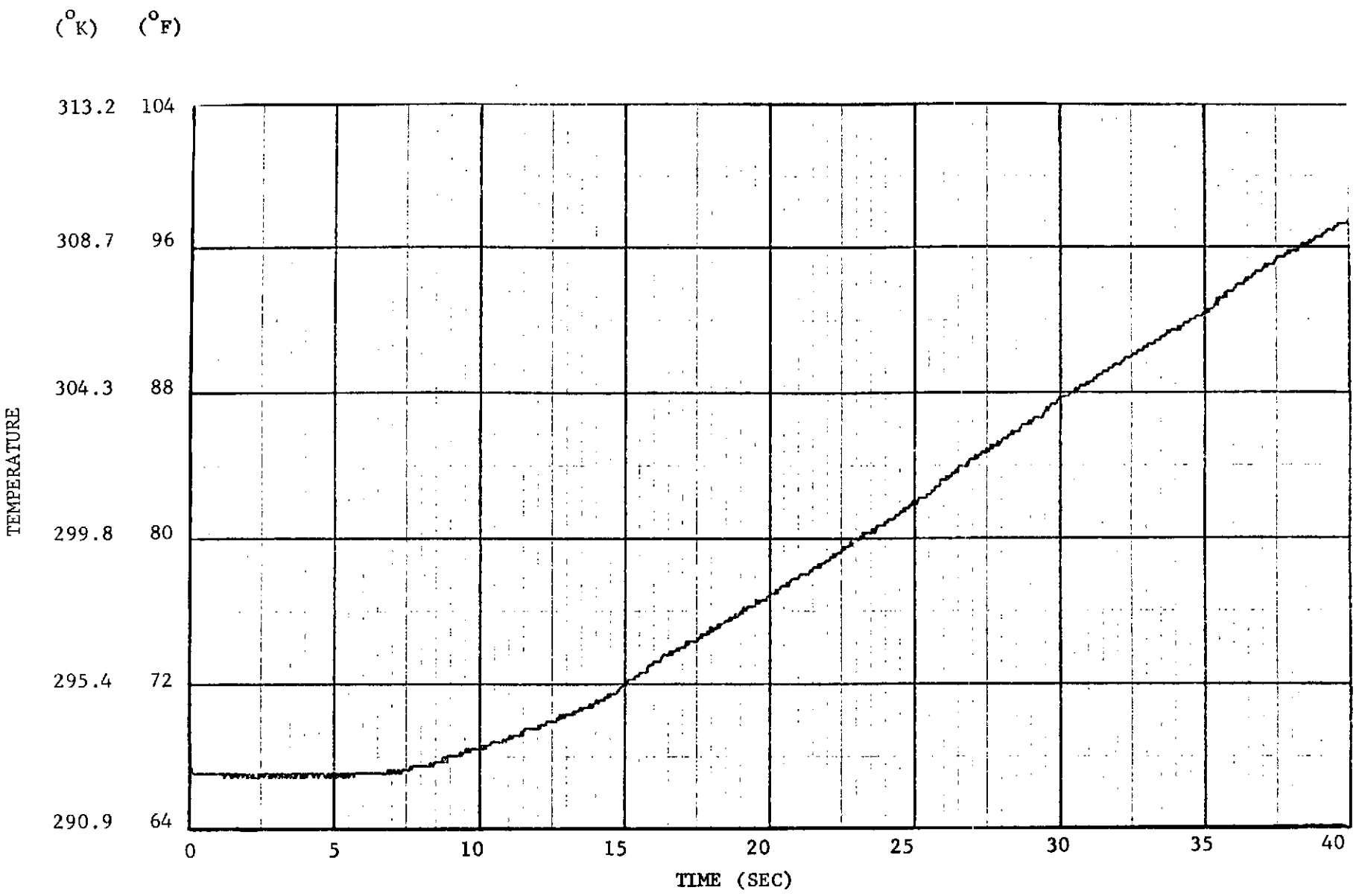

Figure 27. Temperature Versus Time Computer Plot of Thermocouple TCF-2, XJ04/0001

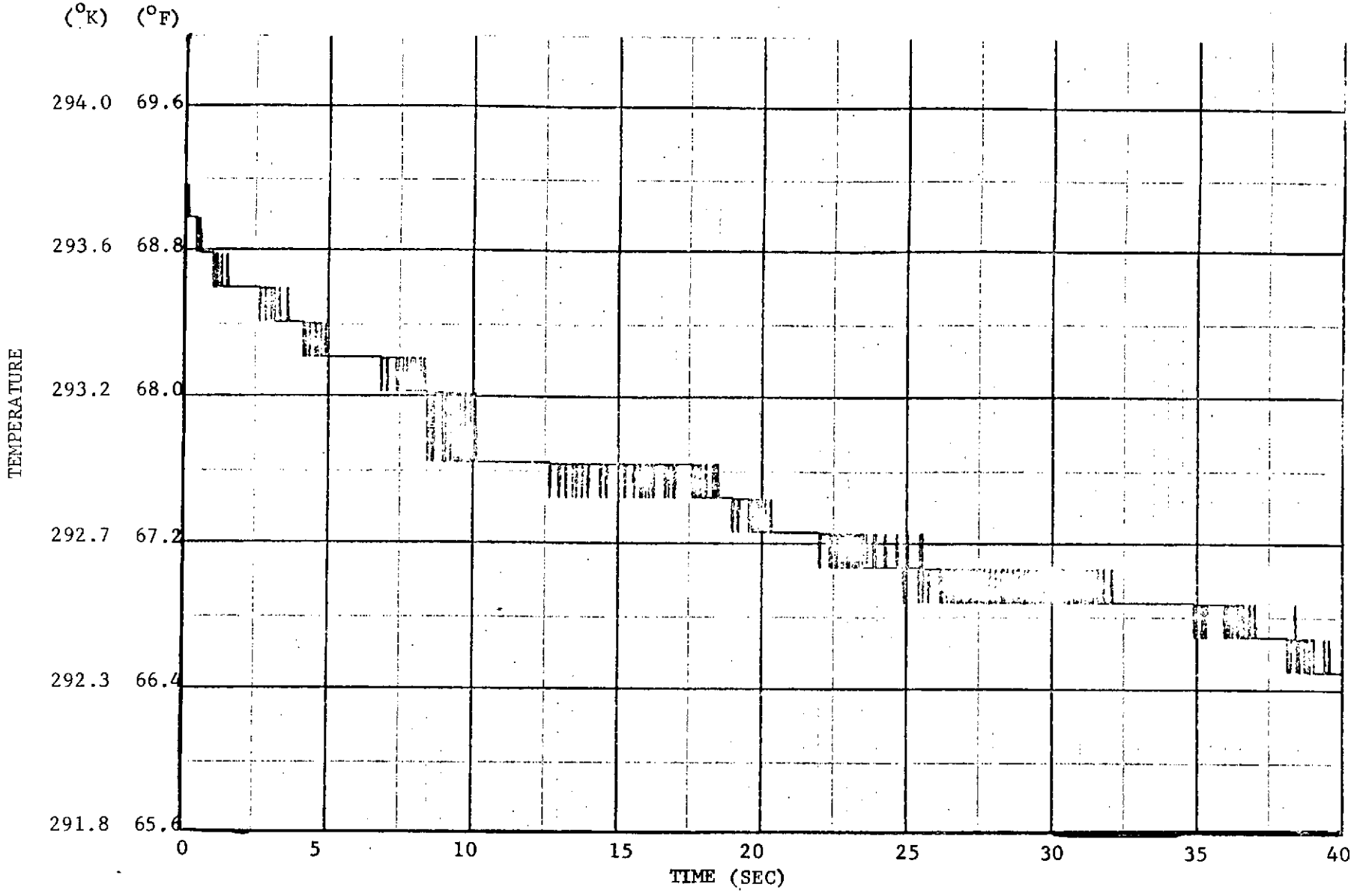

Figure 28. Temperature Versus Time Computer Plot of Thermocuple TCC-3, XJ04/0001

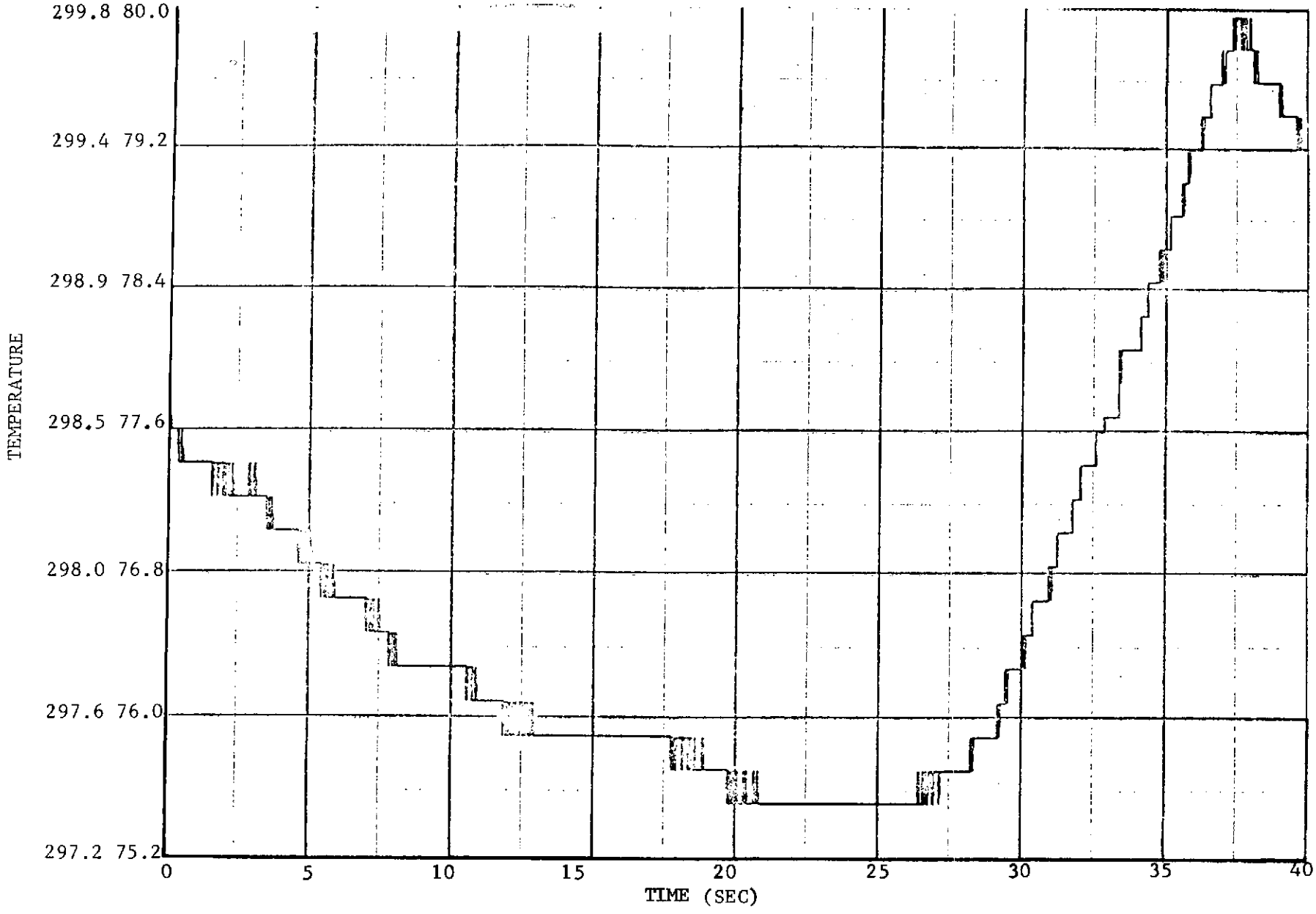

Figure 29. Temperature Versus Time Computer Plot of Thermocouple TCC-4, XJ04/0001

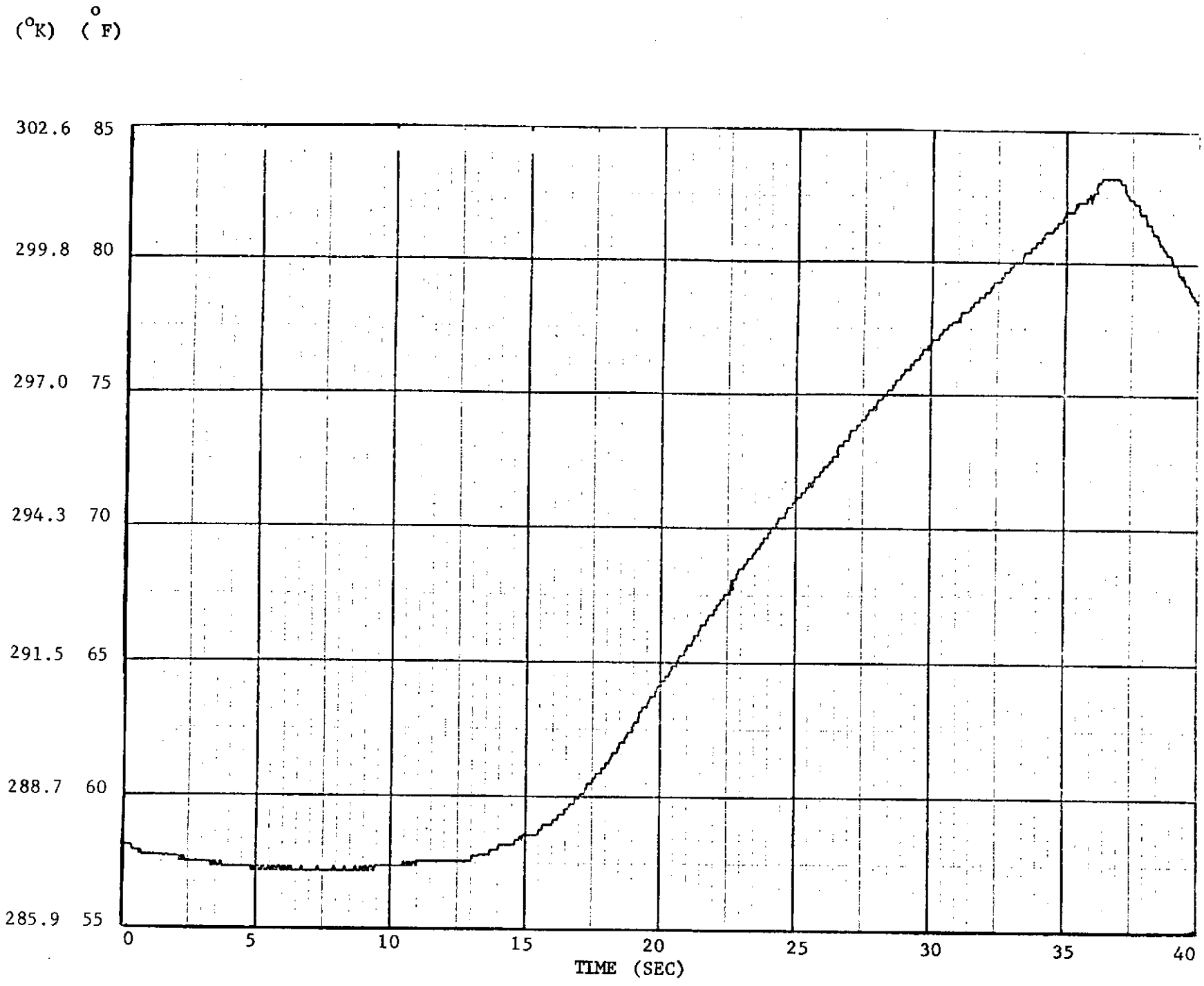

Figure 30. Temperature Versus Time Computer Plot of Thermocouple TCC-5, XJ04/0001

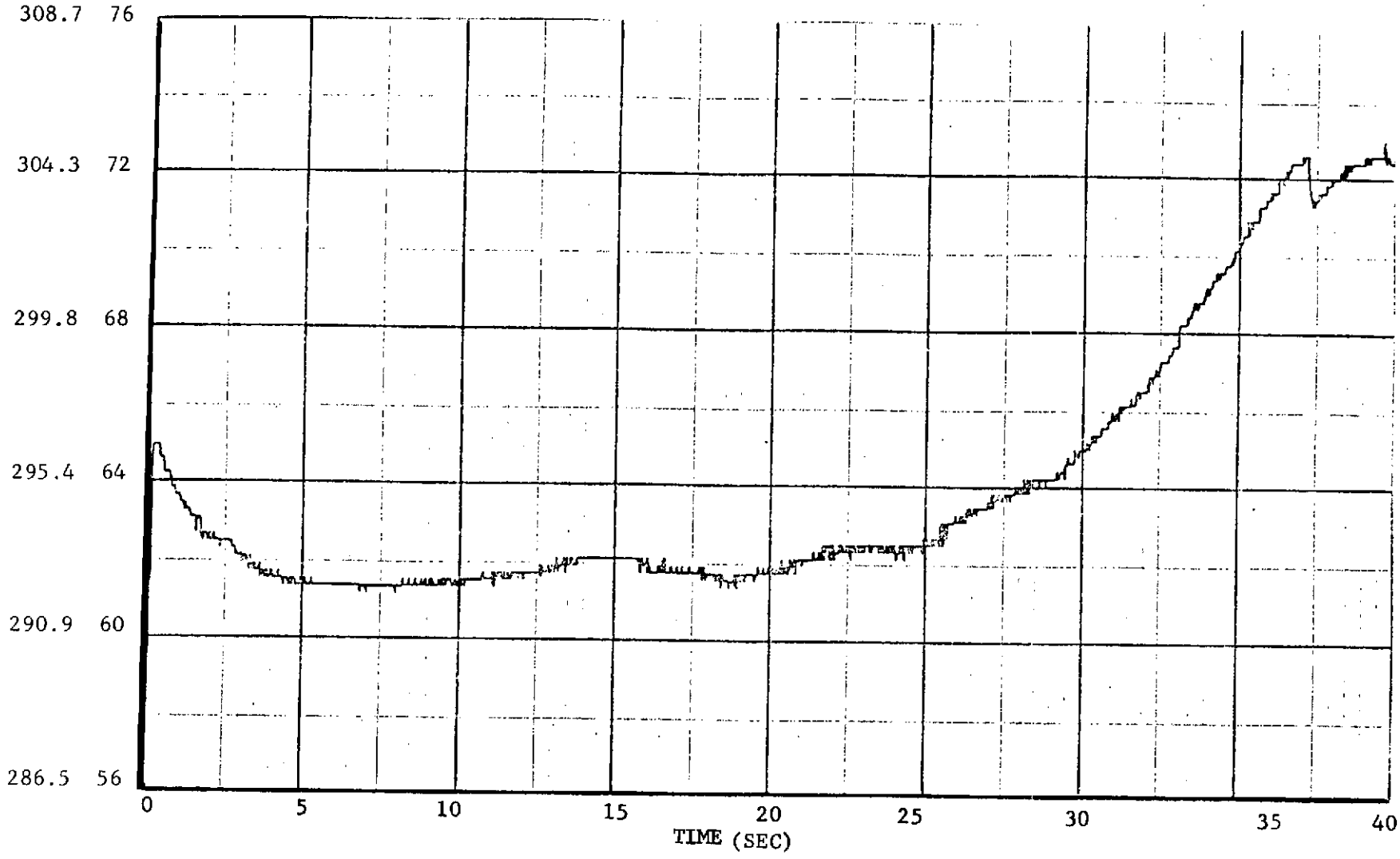

Figure 31. Temperature Versus Time Computer Plot of Thermocouple TCC-6, XJ04/0001

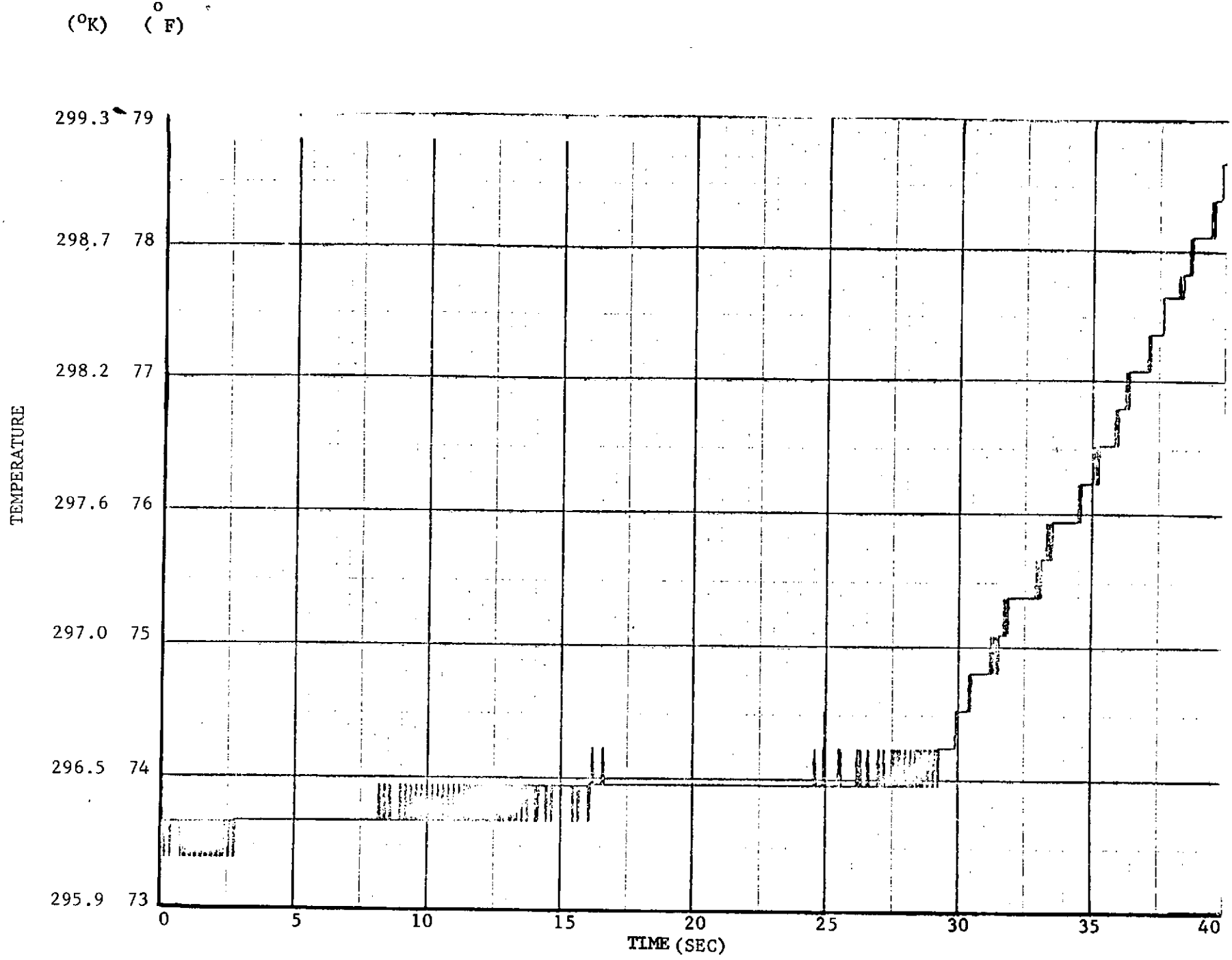

Figure 32. Temperature Versus Time Computer Plot of Thermocouple TCA-7, XJ04/0001

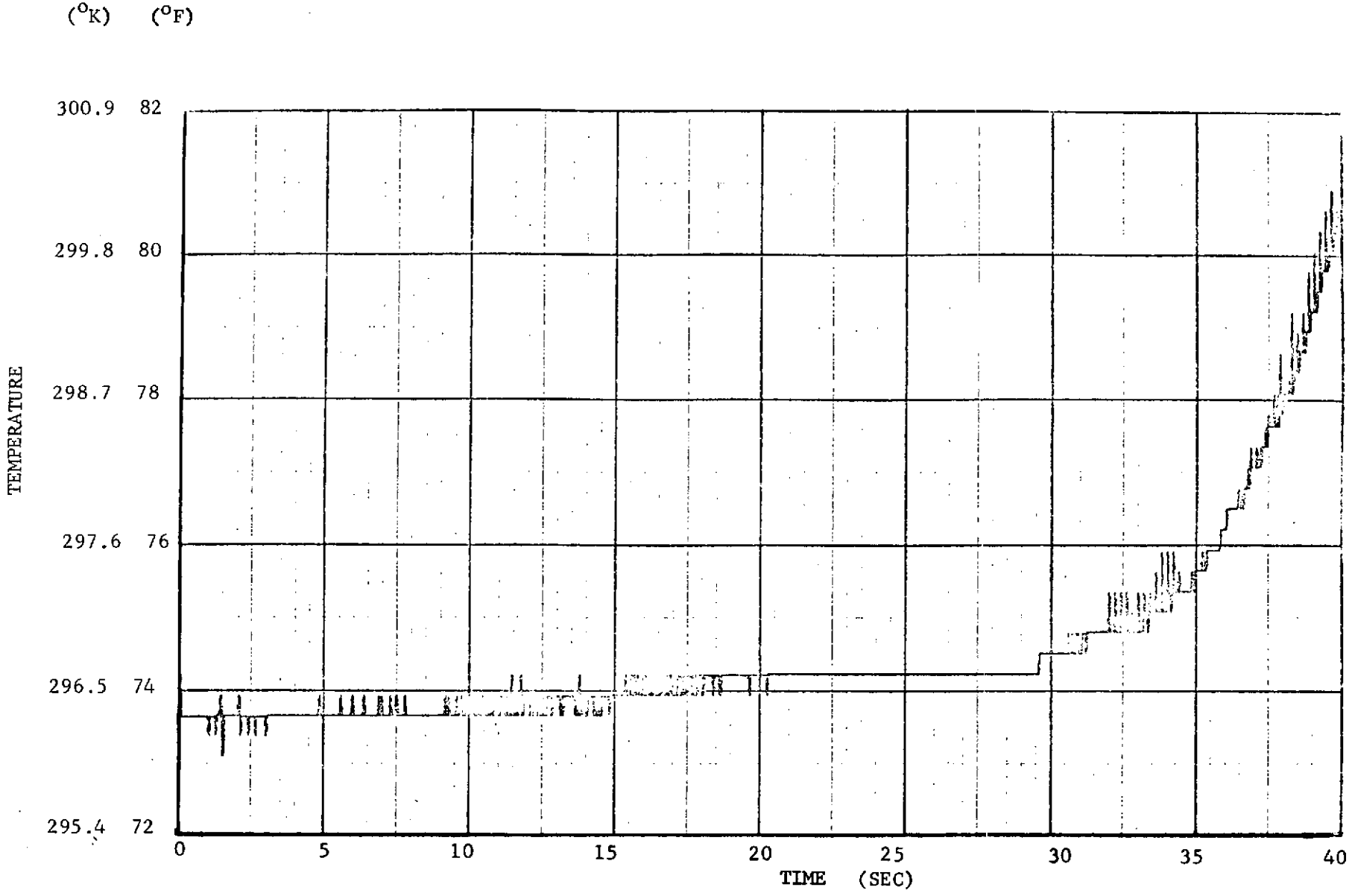

Figure 33. Temperature Versus Time Computer Plot of Thermocouple TCA-8, XJ04/0001

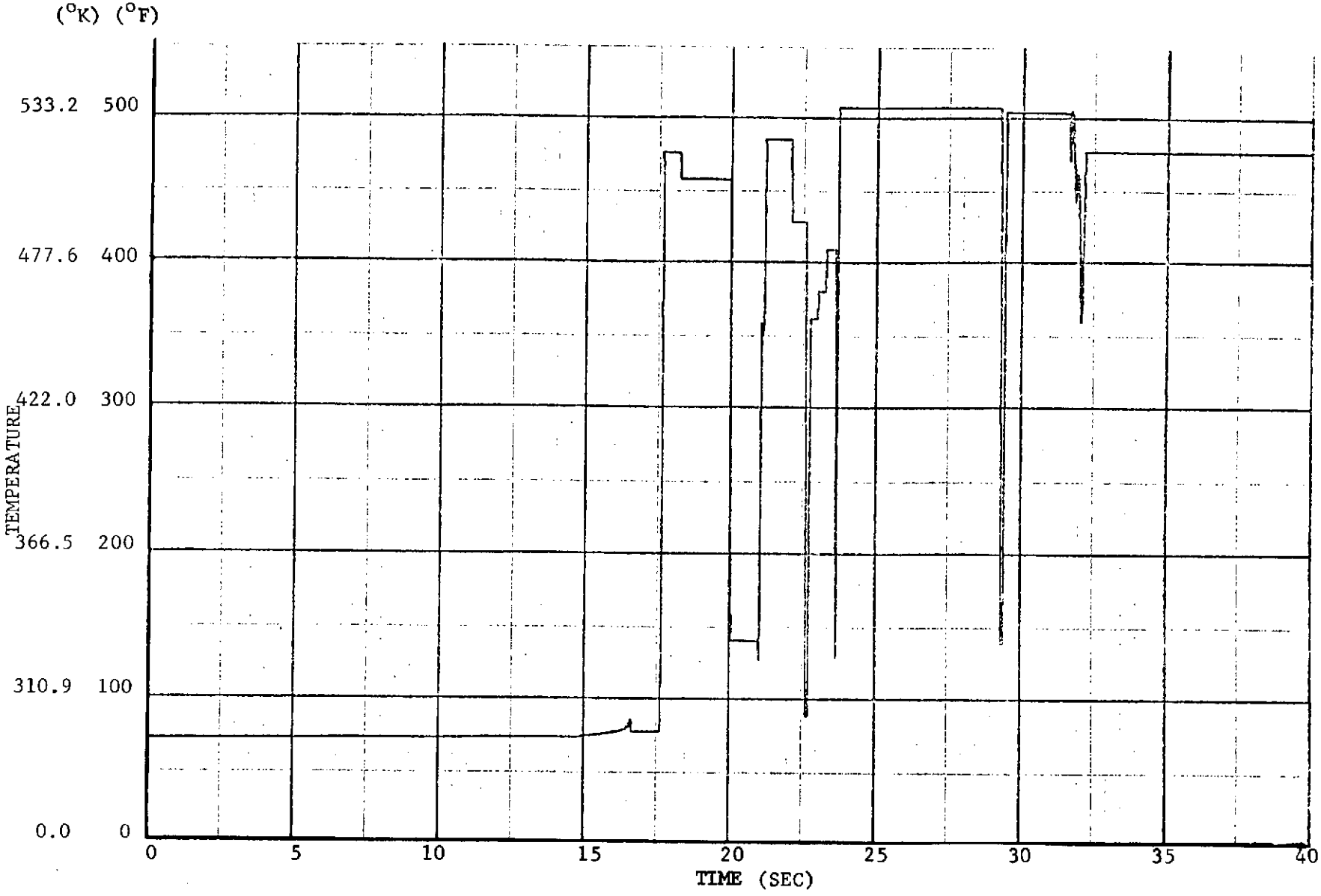

Figure 34. Temperature Versus Time Computer Plot of Thermocouple TNOZ-9, XJ04/0001

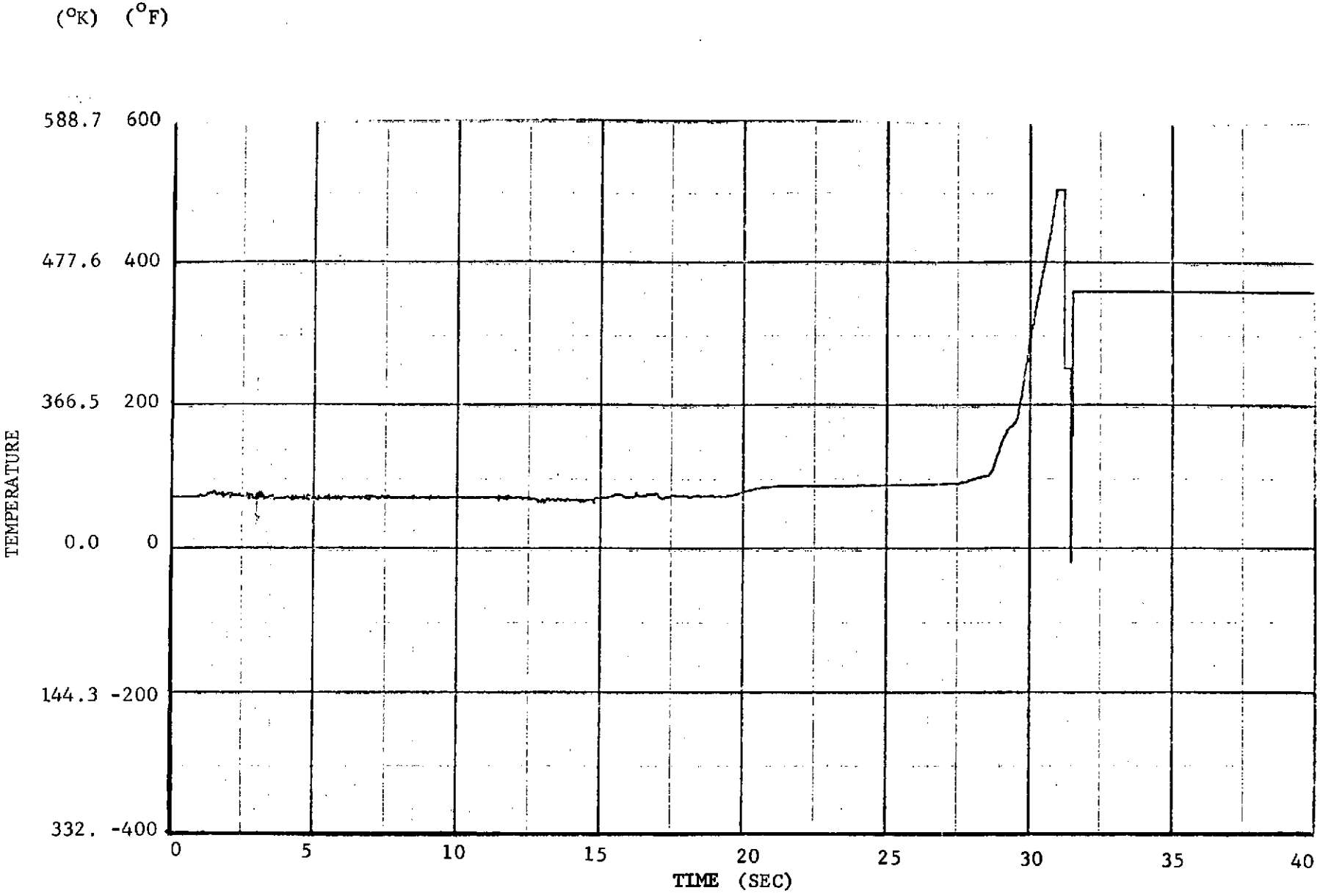

Figure 35. Temperature Versus Time Computer Plot of Thermocouples TNOZ-11, XJ04/0001

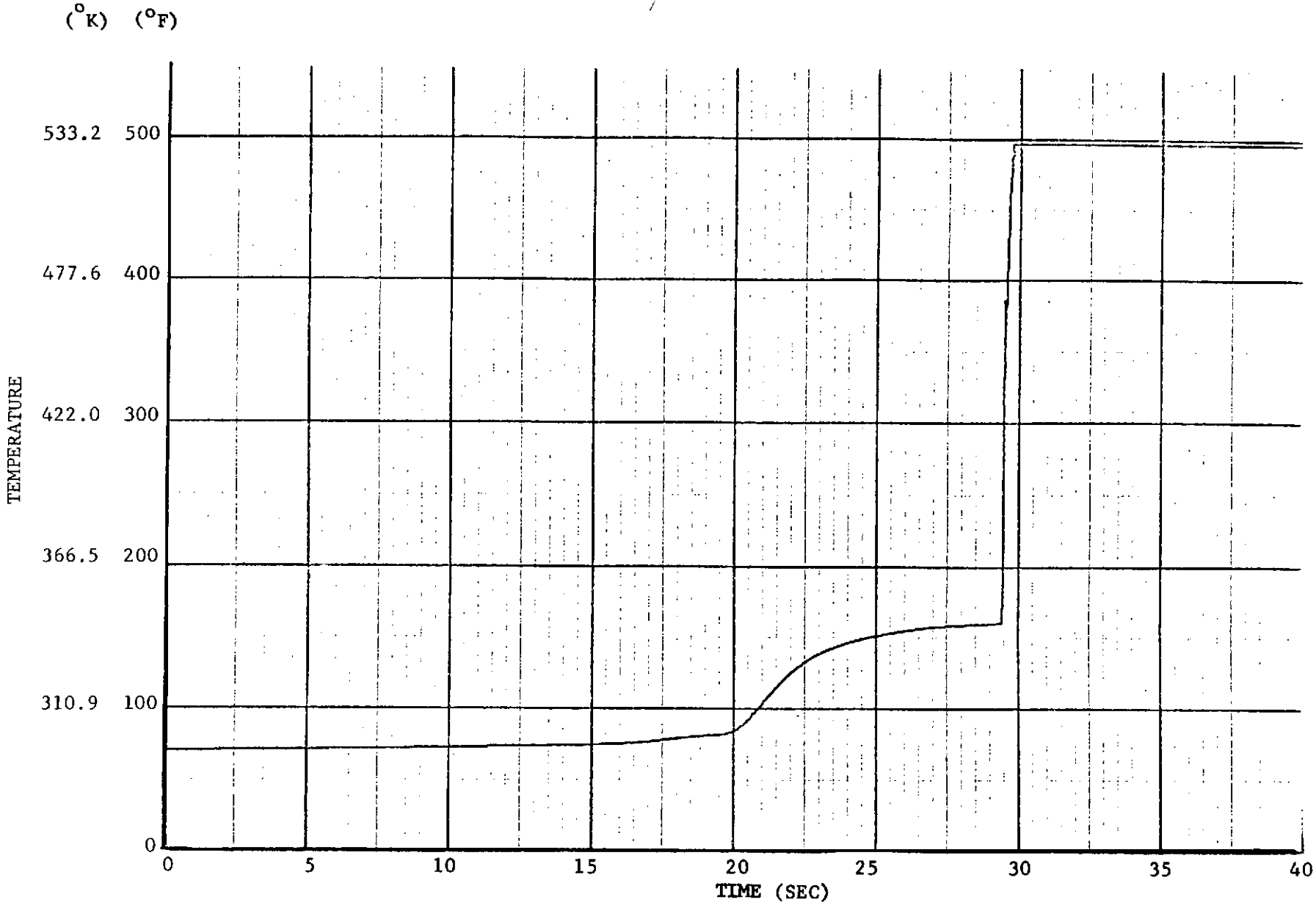

Figure 36. Temperature Versus Time Computer Plot of Thermocouple TNOZ-12, XJ04/0001

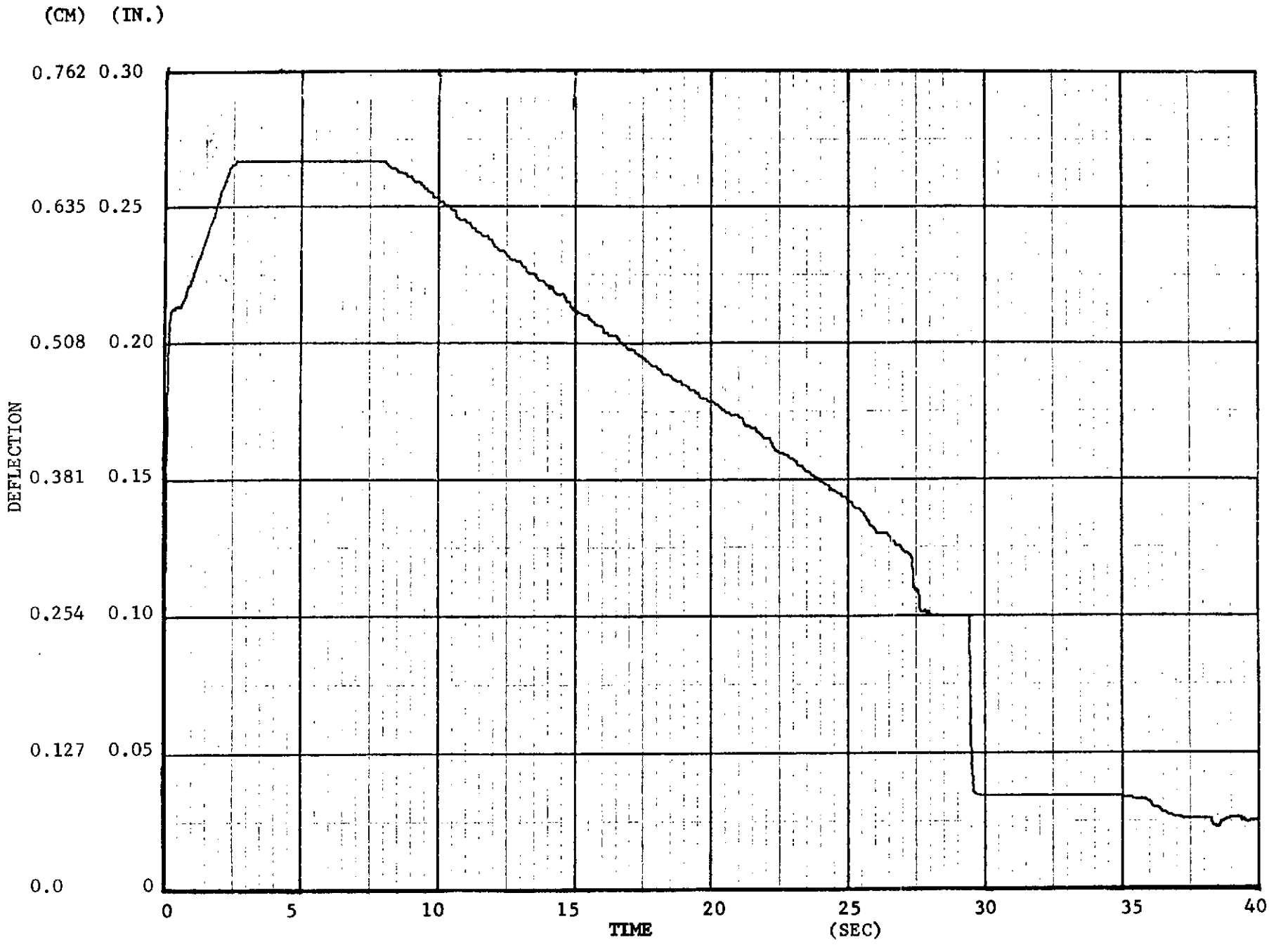

Figure 37. Skirt-To-Skirt Deflection Versus Time Computer Plot of Deflectometer LP-301, XJ04/0001

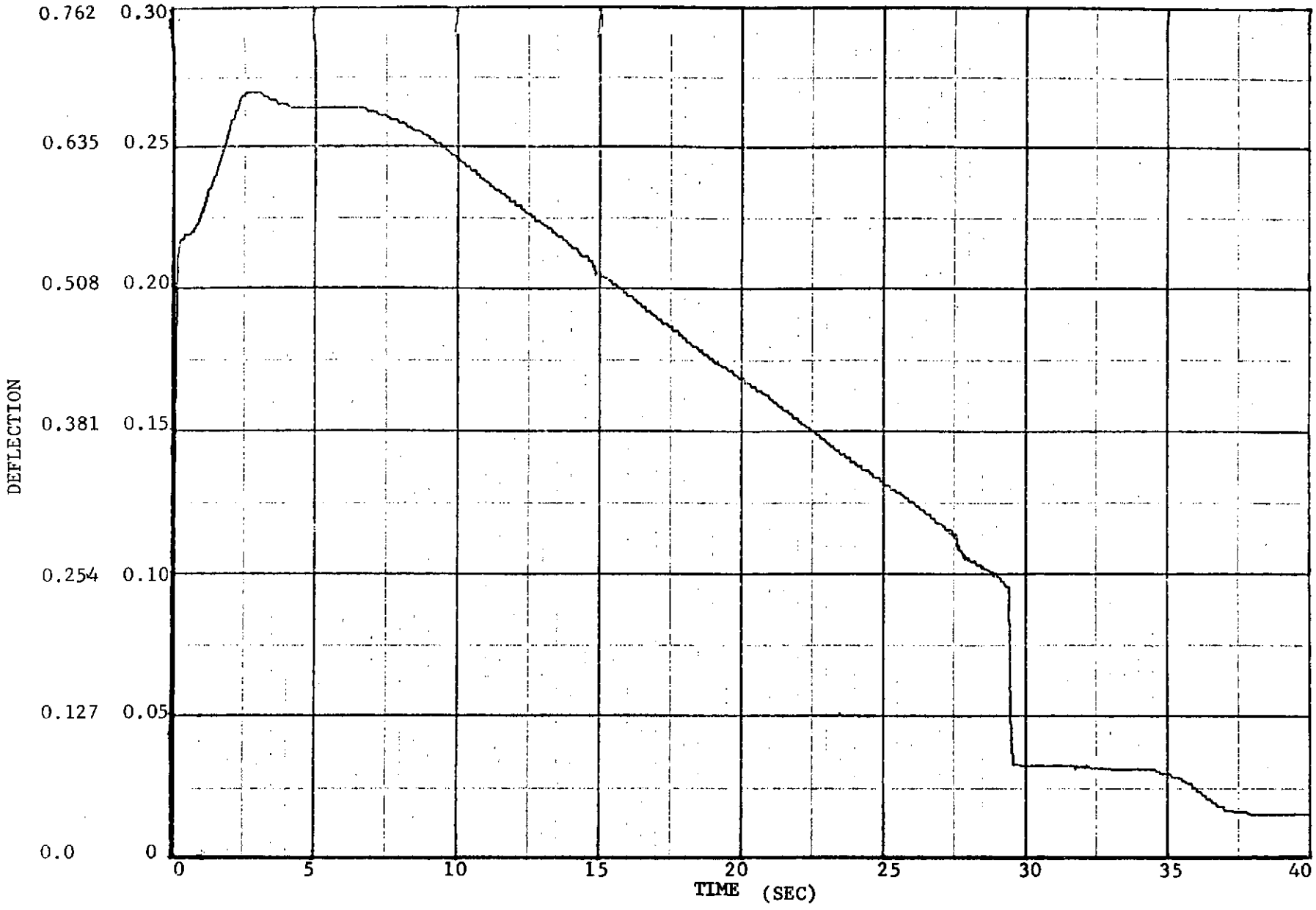

Figure 38. Skirt-To-Skirt Deflection Versus Time Computer Plot of Deflectometer LP-302, XJ04/0001

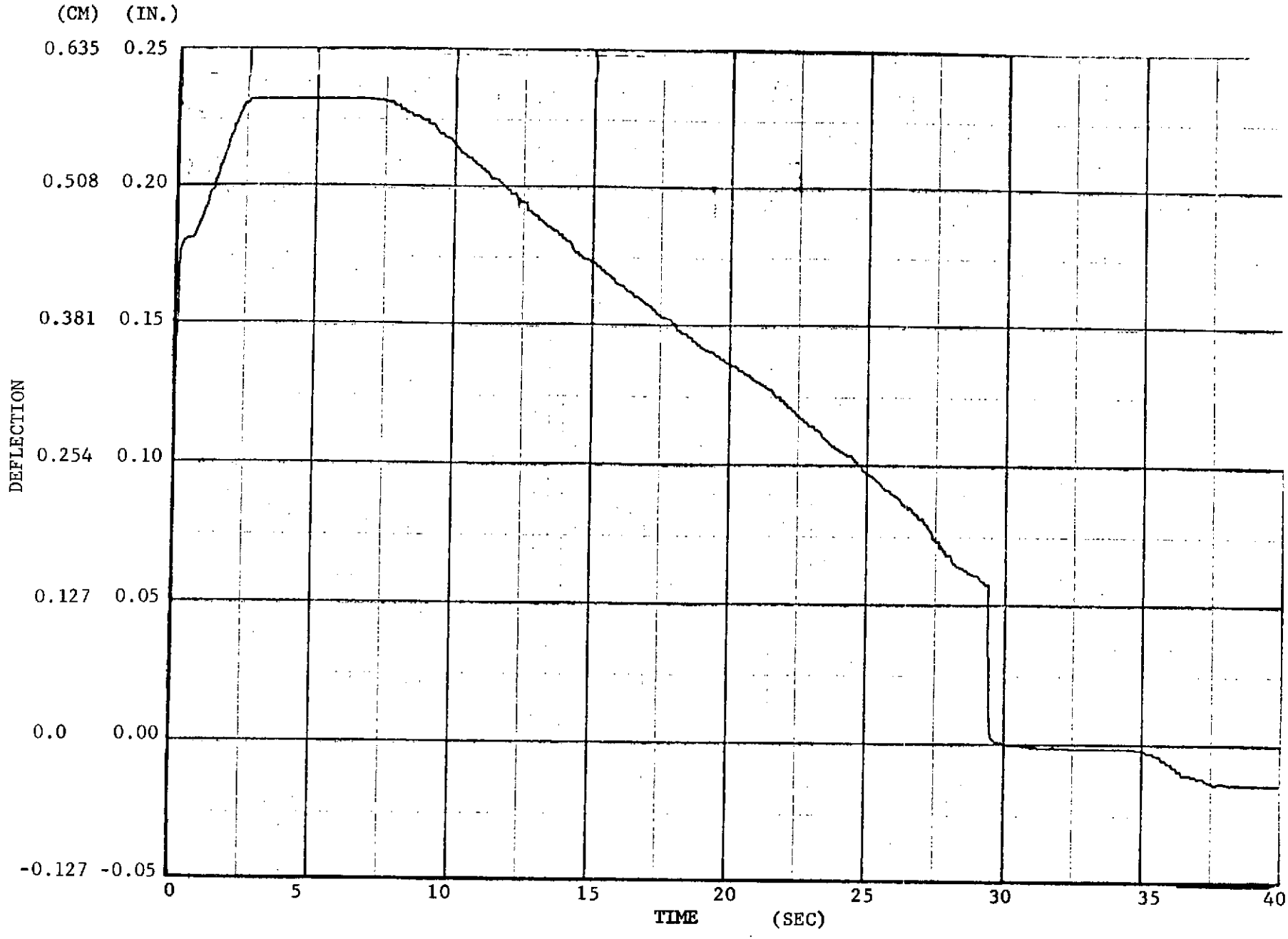

Figure 39. Skirt-To-Skirt Deflection Versus Time Computer Plots of Deflectometer LP-303, XJ04/0001

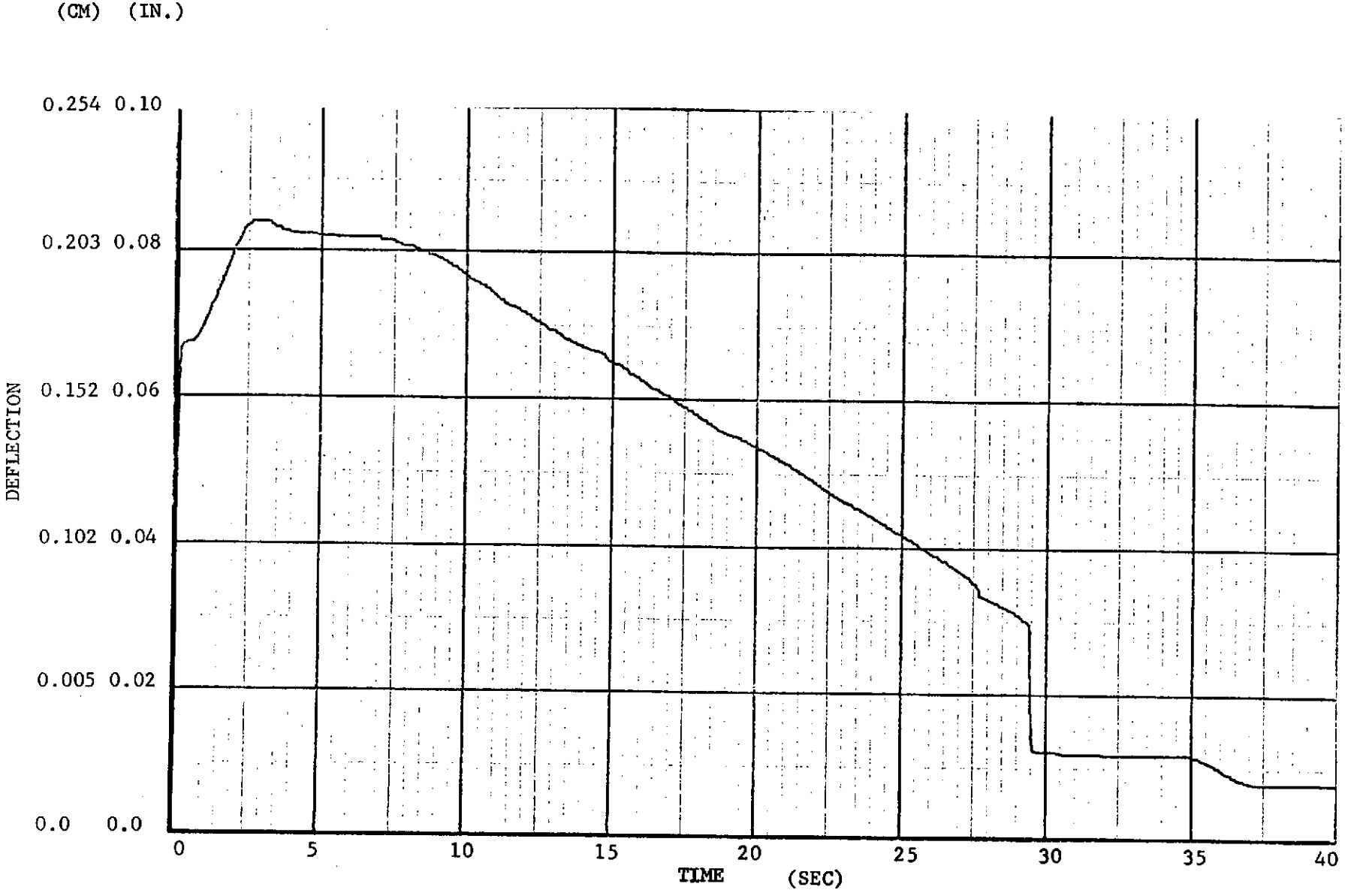

Figure 40. Skirt-To-Skirt Deflection Versus Time Computer Plots of Deflectometer LP-304, XJ04/0001

CONCLUSIONS AND RECOMMENDATIONS

The X259-E6 rocket motor is a modified X259-B4 motor. Differences between the designs include the addition of a forward shrinkage liner, a slightly modified centerbore grain configuration, an adjusted nozzle throat diameter, and the replacement of CYI propellant with an XLDB propellant. Motor serial number XJ04/0001 was fabricated to the X259-E6 design. The XJ04/0001 motor performed satisfactorily except for a nozzle failure. The insulator erosion and char was within expected limits with sufficient insulation remaining to provide a reliable motor design.

The modified centerbore design was not detrimental to the motor firing. In fact, the center core design change resulted in additional propellant being loaded into the chamber.

The nozzle failure is believed to have been caused by a throat insert design that did not function successfully in the severe environment of the XLDB propellant, or because of undetected material imperfections in the throat insert. Motor XJ04/0001 performance data could not be verified because of the nozzle failure. However, the motor firing did provide functional data as shown in the technical sections. The XLDB propellant does perform successfully in the X259-E6 hardware, except for the nozzle, and with a nozzle design change to correct that problem, the motor will perform reliably.

Hercules recommends that the existing X259-B4 nozzles:

(1) Be leak-tested to verify that no leak paths exist

(2) Have the vent holes in the exit cone liner checked for depth to assure that they are not too deep

(3) Have nozzle throat and retainer ring bondlines radiographically inspected to assure adequate adhesive

(4) Have vent holes in the retainer ring filled with adhesive to prevent a possible leak path

All recommendations are of a precautionary nature and are not believed to be the cause of the motor XJ04/0001 nozzle failure.

Hercules also recommends that the nozzle throat for the X259-E6 motor be redesigned and analyzed. A possible configuration for the redesigned nozzle would incorporate a two piece graphite-phenolic throat resulting in a favorable orientation of tape plies in both the converging and diverging sections of the throat insert. Another possible configuration would utilize a monolithic graphite throat of such material as ATJ or ATJS. The redesigned nozzle should be static tested in an X259-E6 motor fabricated to the same design as motor XJ04/0001.

REFERENCES

1. Knuckles, J. W.: Specific Test Plan For Static Firing X259-E6 Antares Motor S/N XJ04/0001 Loaded With High Energy Propellant, Report No. IDS Account No. 07AA023, Hercules Incorporated, Bacchus Works, November 1973.

2. Kordig, J. W.: Engineering Analyses for X259-E6 (Antares II-B) With Demonstration Propellant, Report No. X259/6/40-4031, Hercules Incorporated, Bacchus Works, December 1973.

NASA CR-132557
National Aeronautics and Space Administration.
FINAL REPORT ON THE MANUFACTURE AND STATIC FIRING OF X259-E6 ROCKET MOTOR SERIAL NUMBER XJ04/0001
D. Ray Robertson, Hercules Incorporated, August 1974.
(NASA CONTRACTOR REPORT CR-132557)

Hercules Incorporated, Bacchus Works, loaded high energy crosslinked double base (XLDB) propellant into a standard X259-B4 rocket motor chamber and static tested the motor at the Bacchus Works static test range. The purpose of the firing was to demonstrate the use of XLDB in standard X259 motor hardware. The nozzle was unable to survive the firing, burning through during the motor firing; all other components proved adequate.

I. Robertson, D. Ray
II. Hercules Incorporated
III. NASA CR-132557

NASA

NASA CR-132557
National Aeronautics and Space Administration.
FINAL REPORT ON THE MANUFACTURE AND STATIC FIRING OF X259-E6 ROCKET MOTOR SERIAL NUMBER XJ04/0001
D. Ray Robertson, Hercules Incorporated, August 1974.
(NASA CONTRACTOR REPORT CR-132557)

Hercules Incorporated, Bacchus Works, loaded high energy crosslinked double base (XLDB) propellant into a standard X259-B4 rocket motor chamber and static tested the motor at the Bacchus Works static test range. The purpose of the firing was to demonstrate the use of XLDB in standard X259 motor hardware. The nozzle was unable to survive the firing, burning through during the motor firing; all other components proved adequate.

I. Robertson, D. Ray
II. Hercules Incorporated
III. NASA CR-132557

NASA

NASA CR-132557
National Aeronautics and Space Administration.
FINAL REPORT ON THE MANUFACTURE AND STATIC FIRING OF X259-E6 ROCKET MOTOR SERIAL NUMBER XJ04/0001
D. Ray Robertson, Hercules Incorporated, August 1974.
(NASA CONTRACTOR REPORT CR-132557)

Hercules Incorporated, Bacchus Works, loaded high energy crosslinked double base (XLDB) propellant into a standard X259-B4 rocket motor chamber and static tested the motor at the Bacchus Works static test range. The purpose of the firing was to demonstrate the use of XLDB in standard X259 motor hardware. The nozzle was unable to survive the firing, burning through during the motor firing; all other components proved adequate.

I. Robertson, D. Ray
II. Hercules Incorporated
III. NASA CR-132557

NASA

NASA CR-132557
National Aeronautics and Space Administration.
FINAL REPORT ON THE MANUFACTURE AND STATIC FIRING OF X259-E6 ROCKET MOTOR SERIAL NUMBER XJ04/0001
D. Ray Robertson, Hercules Incorporated, August 1974.
(NASA CONTRACTOR REPORT CR-132557)

Hercules Incorporated, Bacchus Works, loaded high energy crosslinked double base (XLDB) propellant into a standard X259-B4 rocket motor chamber and static tested the motor at the Bacchus Works static test range. The purpose of the firing was to demonstrate the use of XLDB in standard X259 motor hardware. The nozzle was unable to survive the firing, burning through during the motor firing; all other components proved adequate.

I. Robertson, D. Ray
II. Hercules Incorporated
III. NASA CR-132557

NASA